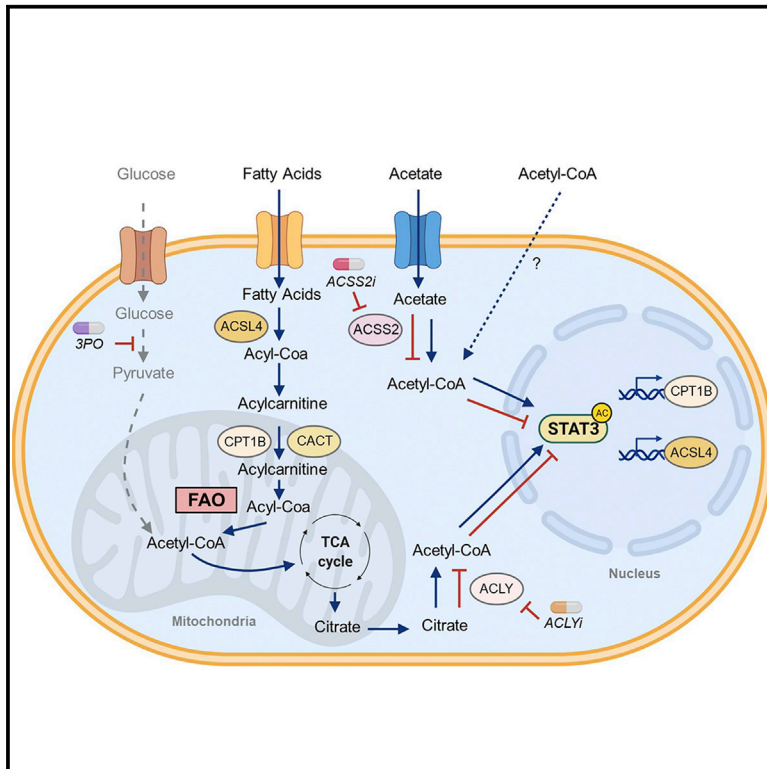


Fatty acid oxidation protects cancer cells from apoptosis by increasing mitochondrial membrane lipids

Graphical abstract



Authors

Yi-Jia Li, Johannes Francois Fahrmann, Maryam Aftabzadeh, ..., David Ann, Samir Hanash, Hua Yu

Correspondence

yili@coh.org (Y.-J.L.),
hyu@coh.org (H.Y.)

In brief

Li et al. demonstrate that FAO mediates chemoresistance in part by acetylating STAT3 through increased acetyl-CoA. Acetylated STAT3 upregulates long-chain acyl-CoA synthetase 4 (ACSL4). Upregulated ACSL4 enhances phospholipid synthesis, which is accompanied by elevated mitochondrial membrane phospholipid levels and strengthened mitochondrial membrane potential. This leads to compromised mitochondrial apoptotic signaling.

Highlights

- Fatty acid oxidation increases acetylated-STAT3 in chemoresistant TNBC cells
- Acetylated STAT3 upregulates ACSL4 to increase phospholipid biogenesis
- Increased phospholipids elevate mitochondrial membrane potential
- Increased mitochondrial membrane potential resists paclitaxel-induced apoptosis



Article

Fatty acid oxidation protects cancer cells from apoptosis by increasing mitochondrial membrane lipids

Yi-Jia Li,^{1,*} Johannes Francois Fahrmann,^{2,7} Maryam Aftabizadeh,^{1,7} Qianqian Zhao,^{1,3} Satyendra C. Tripathi,^{2,6} Chunyan Zhang,¹ Yuan Yuan,⁴ David Ann,^{3,5} Samir Hanash,² and Hua Yu^{1,3,8,*}

¹Department of Immuno-Oncology, Beckman Research Institute and City of Hope Comprehensive Cancer Center, Duarte, CA 91010, USA

²Department of Clinical Cancer Prevention, The University of Texas MD Anderson Cancer Center, Houston, TX 77054, USA

³Irell and Manella Graduate School of Biological Sciences, City of Hope Comprehensive Cancer Center, Duarte, CA 91010, USA

⁴Department of PS Medical Oncology, City of Hope Comprehensive Cancer Center, Duarte, CA 91010, USA

⁵Department of Diabetes Complications and Metabolism, City of Hope Comprehensive Cancer Center, Duarte, CA 91010, USA

⁶Present address: Department of Biochemistry, All India Institute of Medical Sciences, Nagpur, MH, India

⁷These authors contributed equally

⁸Lead contact

*Correspondence: yili@coh.org (Y.-J.L.), hyu@coh.org (H.Y.)

<https://doi.org/10.1016/j.celrep.2022.110870>

SUMMARY

Overcoming resistance to chemotherapies remains a major unmet need for cancers, such as triple-negative breast cancer (TNBC). Therefore, mechanistic studies to provide insight for drug development are urgently needed to overcome TNBC therapy resistance. Recently, an important role of fatty acid β -oxidation (FAO) in chemoresistance has been shown. But how FAO might mitigate tumor cell apoptosis by chemotherapy is unclear. Here, we show that elevated FAO activates STAT3 by acetylation via elevated acetyl-coenzyme A (CoA). Acetylated STAT3 upregulates expression of long-chain acyl-CoA synthetase 4 (ACSL4), resulting in increased phospholipid synthesis. Elevating phospholipids in mitochondrial membranes leads to heightened mitochondrial integrity, which in turn overcomes chemotherapy-induced tumor cell apoptosis. Conversely, in both cultured tumor cells and xenograft tumors, enhanced cancer cell apoptosis by inhibiting ACSL4 or specifically targeting acetylated-STAT3 is associated with a reduction in phospholipids within mitochondrial membranes. This study demonstrates a critical mechanism underlying tumor cell chemoresistance.

INTRODUCTION

Metastatic triple-negative breast cancer (TNBC) has the worst prognosis among all breast cancer subtypes due to acquired chemoresistance. It has become evident that almost all cancer types, including TNBC, reprogram their metabolism to enable neoplastic transformation and tumor progression and therapy resistance (Pavlova and Thompson, 2016). However, the mechanisms underlying chemoresistance associated with elevated lipids remain poorly understood. Recently, fatty acid oxidation (FAO) has received prominent attention for its critical role in progression of several types of cancers, including TNBC (Aloia et al., 2019; Camarda et al., 2016; Carracedo et al., 2013; Chen et al., 2019a; Cheng et al., 2019; Duman et al., 2019; Edmunds et al., 2014; He et al., 2019; Padanad et al., 2016; Pavlova and Thompson, 2016; Qu et al., 2016; Wang et al., 2018). Our previous work demonstrated that JAK/STAT3-regulated carnitine palmitoyltransferase 1 (CPT1)/FAO is critical for TNBC chemoresistance (Wang et al., 2018). However, the mechanisms by which FAO confers TNBC tumor cells with resistance to chemotherapy-induced cell death and apoptosis remain unknown. It is also puzzling how chemoresistant tumor cells replenish acyl-

long-chain fatty acids (LCFAs), which are substrates needed to satiate hyperactive CPT1/FAO.

An elevated phospholipid level is inversely correlated with patient survival (Hattingen et al., 2013). Our previous study demonstrated that phospholipids are elevated in chemoresistant TNBC cells (Wang et al., 2018). Although no clear mechanisms underlying the role of accumulated phospholipids in promoting cancer progression and resistance to therapies have been defined (Hattingen et al., 2013; Ishikawa et al., 2012), phospholipids are abundant in membranous organelles, including mitochondria. Mitochondria are crucial for cellular adaptation to metabolic insults (Crimi and Degli Esposti, 2011; Osman et al., 2011; Tatsuta et al., 2014), and phospholipids (especially lysophosphatidylethanolamines [LPEs] and phosphatidylcholines [PCs]) are the main lipids in mitochondria in addition to other membranous organelles (Gohil and Greenberg, 2009; Mejia and Hatch, 2015; Schenkel and Bakovic, 2014). Cardiolipin (CL), another phospholipid, is found exclusively in the inner mitochondrial membrane (Paradies et al., 2014). Many chemotherapeutics, including paclitaxel and docetaxel, depolarize the mitochondrial membrane potential ($\Delta\psi$) and subsequently activate the mitochondrial apoptotic pathway (Fabbri et al., 2006; Kidd et al., 2002). However, it



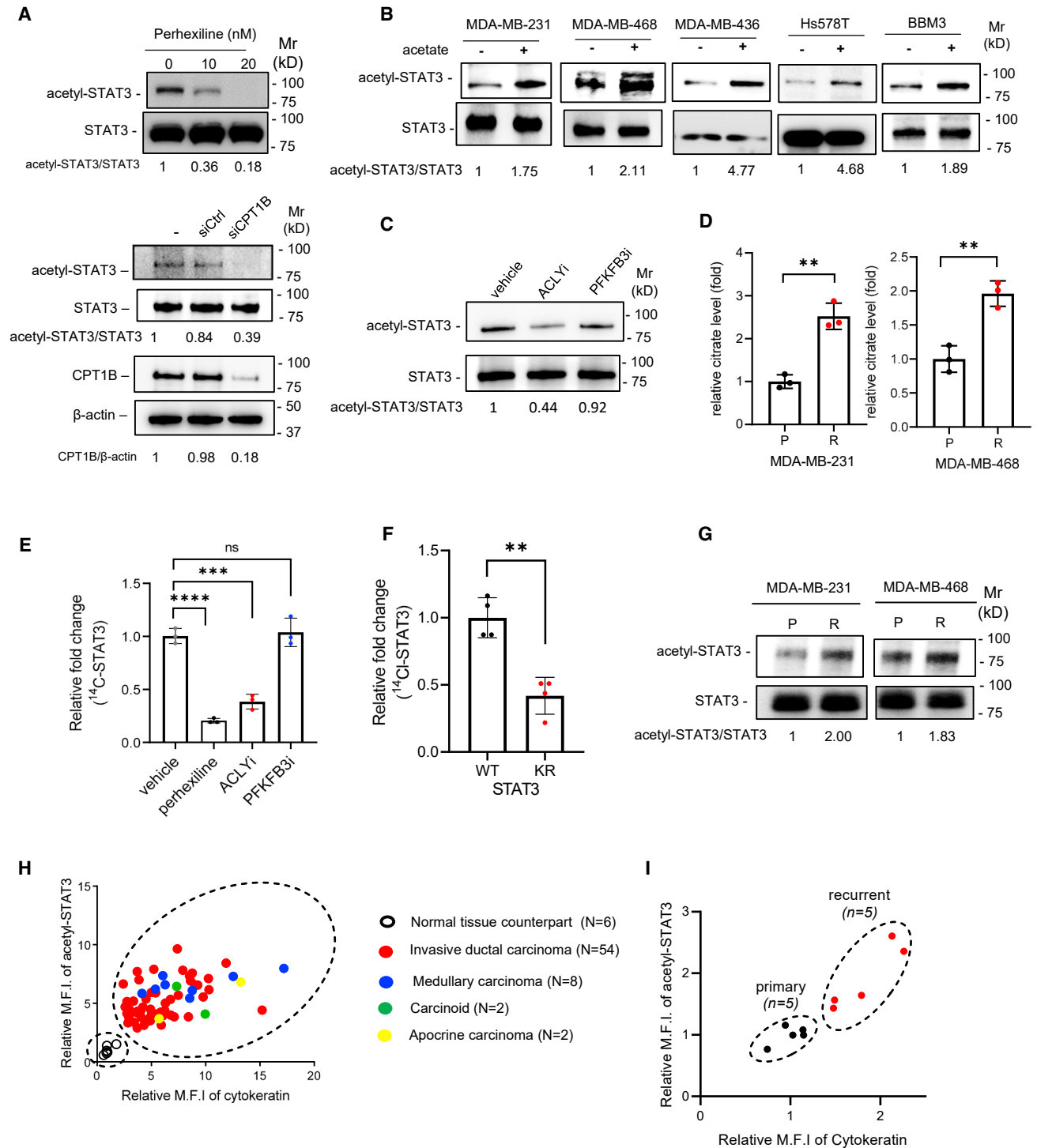


Figure 1. FAO increases acetyl-STAT3 in chemoresistant TNBC via acetyl-CoA

(A) Inhibiting FAO in chemoresistant MDA-MB-231-R cells by perhexiline (upper panels) or CPT1B knockdown suppressed acetylation of STAT3. The level of acetyl-STAT3, total STAT3, CPT1B, and β-actin was assessed by western blotting.

(B) Acetate was added to cultured TNBC cell lines as indicated, and the levels of acetyl-STAT3 and total STAT3 were determined by western blotting.

(C) The levels of acetyl-STAT3 in MDA-MB-231-R cells treated with vehicle, ACLY inhibitor (ACLYi) (BMS-303141), or PFKFB3 inhibitor (PFKFB3i) (3PO) were assessed by western blotting.

(D) Citrate levels were measured in parental (P) and chemoresistant (R) MDA-MB-231 or MDA-MB-468 cells by citrate colorimetric assay.

(legend continued on next page)

remains unclear whether the levels of phospholipids in mitochondrial membranes play a role in anti-apoptosis and chemoresistance.

Multiple recent reports demonstrate a critical role of CPT1, the rate-limiting enzyme for FAO, in cancer progression or chemoresistance (Camarda et al., 2016; Carracedo et al., 2013; Qu et al., 2016; Wang et al., 2018). However, the mechanisms by which CPT1/FAO counteracts apoptosis of chemoresistant cells are unclear. Although NADPH and ATP from FAO likely contribute to resistance to cell death, highly active CPT1/FAO is expected to metabolize activated LCFAs (acyl-coenzyme A [CoA]) necessary for FAO and to produce more ATP to support cancer cell growth. What might be the mechanism that ensures the continuous supply of LCFAs (acyl-CoA) when FAO activity is elevated needs to be explored.

One of the main products of FAO is acetyl-CoA (Edmunds et al., 2014; Houten and Wanders, 2010). In addition to being essential for ATP and NADPH generation, acetyl-CoA is important for protein acetylation (Cai et al., 2011; Comerford et al., 2014; Pougovkina et al., 2014). STAT3 acetylation, especially at K685, has been shown to play a major role in STAT3 activation, oncogenicity, and mitochondrial energy production (Lee et al., 2012; Xu et al., 2016; Yuan et al., 2005).

In this study, we explored the mechanisms by which FAO mitigates tumor cell apoptosis. We found that FAO reprograms phospholipid biosynthesis through acetylated STAT3-mediated upregulation of long-chain acyl-CoA synthetase 4 (ACSL4), which in turn increases phospholipid synthesis and mitochondrial membrane phospholipid levels, leading to heightened mitochondrial $\Delta\psi$ that counteracts the mitochondrial apoptotic pathway.

RESULTS

FAO increases acetylated-STAT3 in chemoresistant TNBC

Our previous study showed chemoresistant MDA-MB-231-R cells exhibit elevated FAO and FAO contributes to chemoresistance in TNBC cells (Wang et al., 2018). Another chemoresistant TNBC cell line, MDA-MB-468-R, also shows accelerated FAO compared with its parental counterpart (Figure S1A). But how FAO may contribute to chemoresistance remains unknown. Since activated STAT3 underlies chemoresistance (Wang et al., 2018), we investigated whether FAO could affect STAT3 acetylation. Blocking FAO by a CPT1 inhibitor, perhexiline, or

knocking down carnitine palmitoyltransferase 1B (CPT1B), a critical enzyme in FAO, reduced STAT3 acetylation at K685 in the chemoresistant TNBC cells (Figure 1A). Supporting the role of FAO in activating STAT3 through acetyl-CoA, supplementing both acetate and synthetic acetyl-CoA to the culture medium increased the level of acetylated (acetyl)-STAT3 in five different TNBC cell lines (Figures 1B and S1B). In addition, acetate and acetyl-CoA induced acetyl-STAT3 in colorectal cancer cells and mouse splenic T cells (Figure S1C). Acetate is converted to acetyl-CoA by acyl-CoA synthetase short chain family member 2 (ACSS2) before being used for protein acetylation in cells (Houston et al., 2020; Yao et al., 2020). Adding an ACSS2 inhibitor significantly decreased the level of STAT3 acetylation induced by acetate (Figure S1D). Furthermore, the level of acetyl-STAT3 was low in K685R-STAT3 (KR) (acetylation-deficient mutant)-expressing cells cultured in medium supplemented with acetate, indicating that K685 is the major acetylation site of STAT3 mediated by FAO-acetyl-CoA (Figure S1D).

Acetyl-CoA produced from FAO can be converted to citrate and shuttled to cytosol. Citrate is further broken down to acetyl-CoA by ATP citrate synthase (ACLY) and subsequently contributes to cytosolic acetyl-CoA pool for cellular function (Qu et al., 2016). In addition to FAO, acetyl-CoA can be generated from pyruvate through glycolysis (Shi and Tu, 2015). To assess whether acetyl-CoA metabolized from FAO is the main source for STAT3 acetylation, we examined the level of acetyl-STAT3 in the presence of either ACLY or glycolysis inhibitor. We found that ACLY inhibitor (ACLYi) (BMS-303141), but not glycolysis inhibitor (6-phosphofructo-2-kinase/fructose-2,6-bisphosphatase isoform 3 inhibitor [PFKFB3] [3PO]), decreased the level of acetyl-STAT3 (Figure 1C). In addition, the level of citrate was elevated in the two chemoresistant TNBC cell lines (Figure 1D), which was decreased after knocking down STAT3 or CPT1B (Figure S1E). In addition to FAO inhibitor (Wang et al., 2018), we found that ACLY inhibitor also decreased MDA-MB-231-R cell proliferation (Figure S1F), suggesting FAO-acetyl-CoA contributes to biomass through proliferation. Further, pyruvate levels in the two chemoresistant TNBC cell lines were only slightly lower than their parental cell lines (Figure S1G). These results are consistent with the notion that acetyl-CoA from FAO is the main source for STAT3 acetylation.

To provide the direct evidence that acetyl-CoA metabolized from increased FAO could lead to acetylation of STAT3, ^{14}C -labeled palmitic acid was added to cultured MDA-MB-231-R cells as a FAO substrate. The results show that, while FAO or

(E) ^{14}C -labeled palmitic acid was used to trace whether acetylation of STAT3 in MDA-MB-231-R cells is FAO dependent. ^{14}C -labeled STAT3 was then measured by immunoprecipitation and scintillation counting.

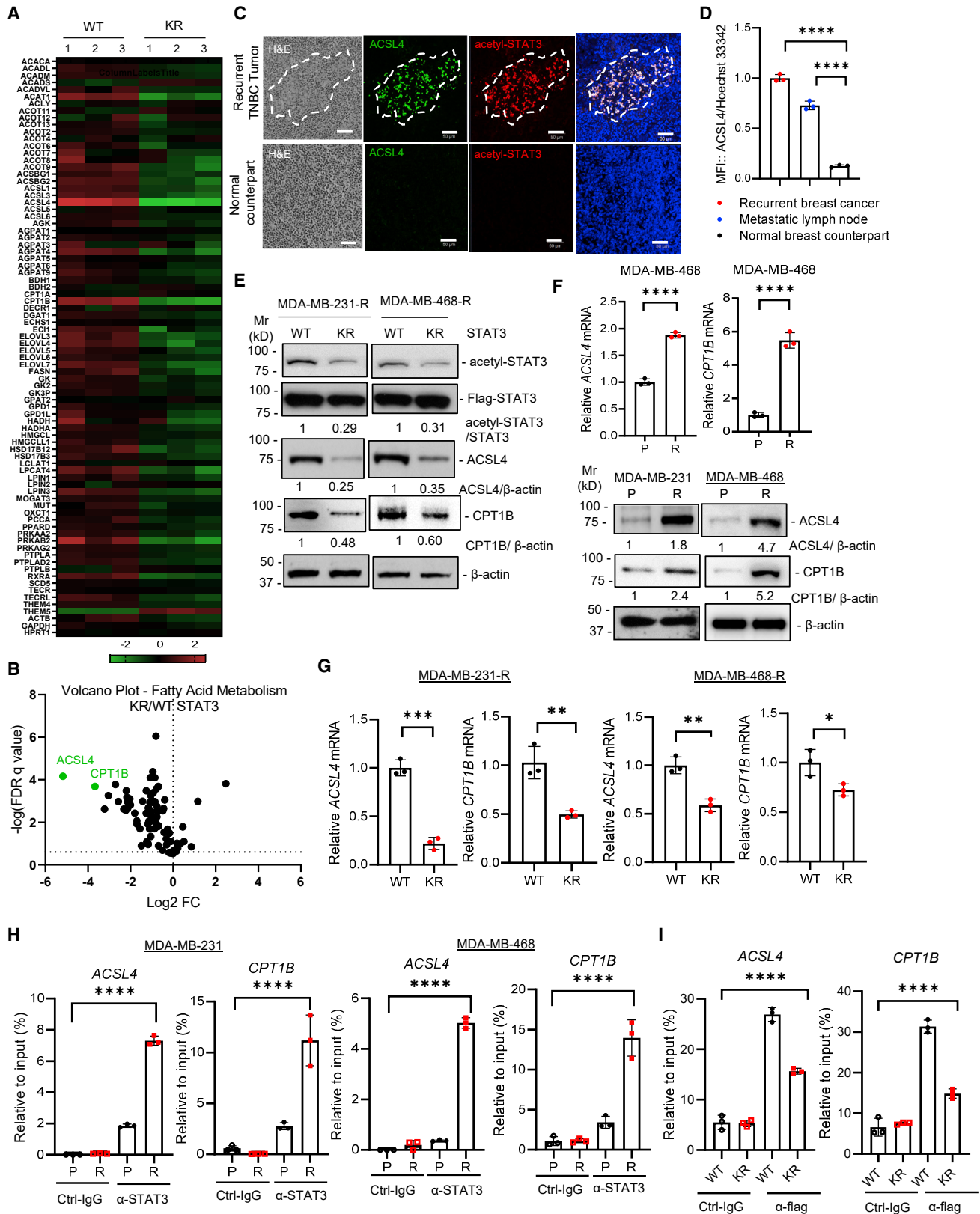
(F) ^{14}C -labeled palmitic acid was used to trace whether acetyl-CoA from FAO is transferred to STAT3. FLAG-tagged wild-type (WT) or K685R mutant STAT3 (KR) was expressed in MDA-MB-231-R cells and used for the lipid-labeling experiment.

(G) The level of acetyl-STAT3 was examined by immunoprecipitation and western blotting in two chemoresistant TNBC cell lines.

(H) Acetyl-STAT3 levels in 66 patient tumor tissues with TNBC on a tumor tissue array including four subtypes as indicated were assessed by fluorescent-immunohistochemistry (IHC) and confocal microscopy. The images of acetyl-STAT3 or cytokeratin were quantified and presented as the mean of fluorescent intensity (M.F.I.). The M.F.I. was then normalized with Hoechst 33342 in the plot.

(I) Acetyl-STAT3 is elevated in patient tumor tissues with recurrent TNBC compared with their primary tumors prior to chemo-treatment shown by IHC staining and quantified as described above. The protein levels of acetyl-STAT3 or CPT1B in this figure were quantified by band intensity of western blotting using ImageJ software and normalized with the level of total STAT3 or β -actin as indicated.

For the bar graph in (D) and (F), data shown are mean \pm SD; (D and E) $n = 3$; (F) $n = 4$; $n =$ biological replicates; two tailed and unpaired Student's t test; ns, not significant; ** $p < 0.01$; *** $p < 0.05$; **** $p < 0.001$. See also Figure S1 and Table S1A.



(legend on next page)

ACLYi treatment decreased the level of ^{14}C -labeled STAT3, PFKFB3i did not (Figure 1E). Further, ^{14}C -labeled palmitic acid was added to the cultured cells expressing either wild-type (WT) or KR-STAT3. We found the level of ^{14}C -labeled STAT3 was significantly decreased in KR-STAT3-expressing cells (Figure 1F).

To evaluate whether FAO-acetyl-CoA-mediated STAT3 acetylation has an important role in TNBC chemoresistance, we examined acetyl-STAT3 levels in the chemoresistant TNBC cell lines, MDA-MB-231-R and MDA-MB-468-R, compared with their parental cell lines (Figure 1G). Consistent with their high FAO rate (Figure S1A), the level of acetyl-STAT3 was elevated (Figure 1G). Furthermore, STAT3 acetylation at K685 was also significantly elevated in human invasive TNBC tumor tissues ($n = 66$) compared with normal tissue counterparts (Figures 1H and S1H). Importantly, in five paired primary and recurrent TNBCs, after chemotherapy, acetyl-STAT3 was higher in chemoresistant compared with primary tumors (Figures 1I and S1I).

Acetylated STAT3 upregulates ACSL4

Differential gene expression data and volcano plot from acetylation-deficient KR-STAT3-expressing cancer cells indicate that acetylation of STAT3 regulates lipid metabolic genes, including ACSL4 and CPT1B (Figures 2A and 2B). ACSL4 expression was highly elevated in recurrent TNBC tumor tissues with increased acetyl-STAT3 levels (Figure 2C). Also, ACSL4 was highly expressed in all three recurrent, chemoresistant TNBC tumors and lymph node metastases examined (Figures 2D and S2A). Furthermore, expression of FAO and ACSL genes was significantly increased in various patient databases on invasive TNBC (Figure S2B). Expression of both CPT1B and ACSL4 was decreased in KR-STAT3-expressing chemoresistant TNBC cells (Figure 2E).

Importantly, the chemoresistant MDA-MB-231-R and MDA-MB-468-R exhibited elevated gene expression of ACSL4 in addition to CPT1B (Figure 2F; Wang et al., 2018). Overexpressing KR-STAT3 significantly reduced expression of both ACSL4 and

CPT1B genes in the chemoresistant cell lines (Figures 2E and 2G). Chromatin immunoprecipitation (ChIP) assay revealed a higher level of STAT3 bound to the promoters of ACSL4 and CPT1B, but not other FAO and ACSL genes, in the two chemoresistant and one stem-cell-enriched TNBC cell lines tested (Figures 2H and S2C). Furthermore, ChIP assays using cells expressing WT or KR-STAT3 showed that acetyl-STAT3 regulates ACSL4 and CPT1B transcriptionally (Figure 2I).

To further validate the FAO/acetyl-CoA-acetyl-STAT3-ACSL4 pathway delineated above, we inhibited FAO. FAO inhibition reduced STAT3 acetylation at K685 (Figure 1A) and expression of ACSL4 and CPT1B (Figure 3A). In addition, ectopic expression of CPT1B in parental TNBC cells led to the accumulation of acetyl-CoA (Figures 3B and S3A). Conversely, blocking FAO by etomoxir or perhexiline or silencing STAT3 or CPT1B in MDA-MB-231-R cells decreased acetyl-CoA abundance (Figures 3C and S3B). Adding acetate or acetyl-CoA to cultured TNBC cells increased expression of ACSL4 and CPT1B (Figures 3D and S3C).

STAT3 is well known to regulate genes important for cell survival and proliferation. We therefore examined the effects of KR-STAT3 on expression of cell-proliferation genes in the chemoresistant TNBC cells (Figure S3E).

ACSL4-mediated phospholipid biogenesis upregulates mitochondrial $\Delta\psi$

A central question is how accelerated FAO in TNBC chemoresistant cells counteracts apoptosis. Our previous study demonstrated that LCFA can be supplied to TNBC cells by adipocytes and that phospholipids are elevated in chemoresistant TNBC cells (Wang et al., 2018). To demonstrate that phospholipid content is regulated by STAT3 and ACSL4, we performed tandem mass spectrometry (MS/MS) analyses in both positive and negative ion modes, which showed that the phospholipid content of a wide range of species of PC and CL in the cell membranes of the chemoresistant TNBC cells was significantly decreased by silencing STAT3 (Figure 4A). Only one species of PE

Figure 2. ACSL4 is upregulated by acetyl-STAT3 and elevated in patients with chemoresistant TNBC tumors

- (A) The heatmap showing differential expression of fatty acid metabolic genes in MDA-MB-231-R cells expressing WT or KR-STAT3. Data ($n = 3$ independent assays) are shown by \log_2 fold changes. -2 to $+2$, green-to-red color key indicates the intensity associated with normalized expression values.
- (B) Volcano plot depicting differentially expressed genes described in (A) showing the significant downregulation of ACSL4 and CPT1B in KR-expressing MDA-MB-231-R cells. y axis denotes $-\log_{10}$ false discovery rate (FDR) q values, while x axis shows \log_2 fold change values. Volcano plot was generated using GraphPad Prism.
- (C) IHC staining shows acetyl-STAT3 and ACSL4 are elevated in patient tumor tissues with recurrent TNBC compared with their adjacent normal counterparts. White dashed line indicates the tumor tissue. Scale bars, $50 \mu\text{m}$.
- (D) ACSL4 protein expression is upregulated in recurrent breast cancer and the nearby lymph nodes of the metastatic TNBC tumors. The graph presents the ratio of M.F.I. for ACSL4 and Hoechst 33342 in three lymph nodes or breast tissue samples shown in Figure S2A.
- (E) The levels of acetyl-STAT3, CPT1B, and ACSL4 were assessed by western blotting in two TNBC cell lines with ectopic expression of FLAG-tagged WT or KR-STAT3.
- (F) Gene (upper panels) and protein (lower panels) expression of ACSL4 and CPT1B was assessed in (P) and (R) TNBC cells. The level of gene expression in chemoresistant cells was normalized with parental cells.
- (G) Acetylation of STAT3 is necessary for ACSL4 and CPT1B expression in chemoresistant TNBC cells as examined by qPCR.
- (H) ChIP-qPCR showed STAT3 directly binds to the promoters of ACSL4 and CPT1B genes in TNBC cell lines. ChIP with immunoglobulin G (IgG) was performed as negative control.
- (I) Acetylation of STAT3 is required for transcriptional activation of ACSL4 and CPT1B genes. FLAG-tagged WT or KR-STAT3 was overexpressed in MDA-MB-231-R cells. Anti-FLAG antibody was used for ChIP-qPCR. Control IgG was used as a control. The protein levels of acetyl-STAT3, CPT1B, or ACSL4 were quantified as described in Figure 1.
- For the bar graph in (D), (F) and (I), data are shown as mean \pm SD; $n = 3$; two-tailed and unpaired Student's t test; * $p < 0.05$; ** $p < 0.01$; *** $p < 0.005$; **** $p < 0.001$. All ChIP-qPCR results in (H) and (I) were normalized to the total input DNA. Data shown are mean \pm SD; $n = 3$; one-way ANOVA, **** $p < 0.001$. See also Figure S2 and Tables S1B and S2B–S2D.

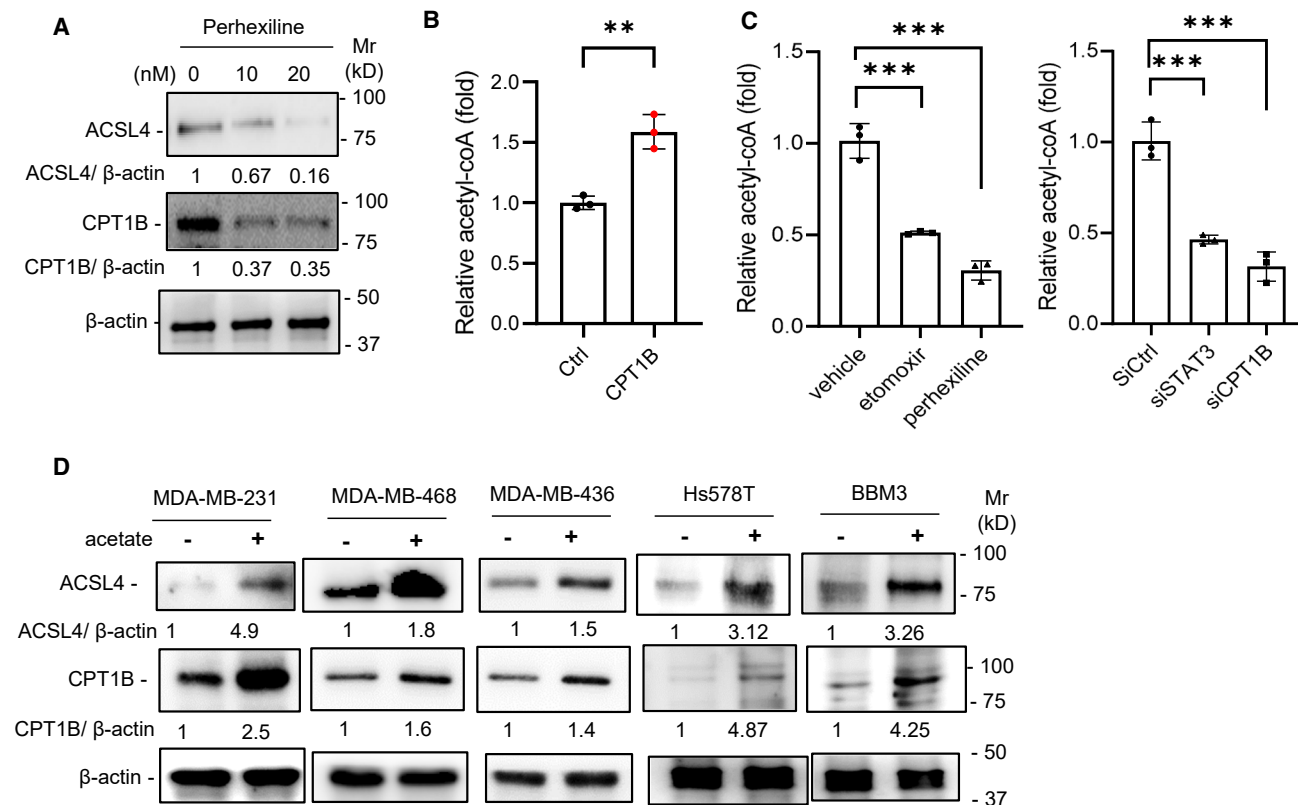


Figure 3. FAO-acetyl-CoA activates STAT3 by acetylation

(A) Perhexiline treatment as described in Figure 1A suppressed the protein expression of ACSL4 and CPT1B, as assessed by western blotting. (B) The levels of acetyl-CoA in parental MDA-MB-231 cells with or without ectopic expression of CPT1B were measured by acetyl-CoA fluorometric assay. (C) The level of acetyl-CoA in MDA-MB-231-R cells under vehicle or FAO inhibitor treatment (left panel) or with STAT3 or CPT1B knockdown by siRNA (right panel) was measured by acetyl-CoA fluorometric assay. Control siRNA (siCtrl) was used as a control. (D) Acetate was added to five different cultured TNBC cell lines, and the expression of ACSL4 and CPT1B was assessed by western blotting. The protein levels of CPT1B or ACSL4 in this figure were quantified as in Figure 1. For the bar graph in (B) and (C), data shown are mean \pm SD; n = 3; two tailed and unpaired Student's t test; **p < 0.01; ***p < 0.05. See also Figure S3 and Table S1C.

phospholipid (36:4) was lower in the same STAT3 knockdown sample (Figure 4A). Similarly, phospholipid content changes of PC, PE, and CL were observed in the cells with ACSL4 gene knockdown (Figure S4A). Since acetyl-STAT3 is required for expression of ACSL4 and FAO genes, we next examined whether mutating acetyl-STAT3 altered phospholipid contents. Thin-layer chromatography (TLC) showed that the total levels of phospholipid were reduced in cells expressing KR-STAT3, with PC and CL decreased significantly while the reduction in PE was less pronounced (Figures 4B and S4B).

While PC and PE have been shown to be the most abundant phospholipids in all mammalian cell membranes (van der Veen et al., 2017), PC, PE, and CL are found predominantly (~90%) in the inner mitochondrial membrane (Daum, 1985; Zinser et al., 1991). We next assessed whether changes in phospholipid contents would affect mitochondrial depolarization. We first silenced STAT3 and ACSL4 and blocked FAO with a CPT1 inhibitor. Inhibiting STAT3, ACSL4, or FAO induced mitochondrial depolarization, as demonstrated with JC1 staining in the MDA-MB-231-R cells (Figures 4C, 4D, and S4C). JC-1 is commonly used to

measure mitochondrial $\Delta\psi$ by the ratio of JC-1 red to JC-1 green (Perelman et al., 2012; Sivandzade et al., 2019; Smiley et al., 1991). The results indicate that STAT3 and ACSL4 are required for maintenance of phospholipid content and mitochondrial $\Delta\psi$ in the chemoresistant TNBC cells (Figures 4C, 4D, and S4C).

Although the concentration of doxycycline we used to induce short hairpin RNA (shRNA) knockdown of STAT3 and ACSL4 was relatively low (2 μ g/mL), doxycycline has been reported to decrease mitochondrial $\Delta\psi$ in A549 or fibroblast cells under daily treatment at 10 μ g/mL concentration (Dijk et al., 2020). To increase scientific rigor, we tested the effects of increasing doxycycline concentrations on mitochondrial $\Delta\psi$ in the chemoresistant TNBC and pancreatic cancer cell lines. Doxycycline only at very high concentrations (>20 μ g/mL) decreased mitochondrial $\Delta\psi$ (Figure S4D). We also confirmed the critical roles of ACSL4 and STAT3 in maintaining mitochondrial $\Delta\psi$ by non-doxycycline-based small interfering RNA (siRNA) knockdown (Figures S4E and S4F).

To rule out that reduced mitochondrial mass might affect mitochondrial $\Delta\psi$, mitochondrial DNA (mtDNA) was measured and

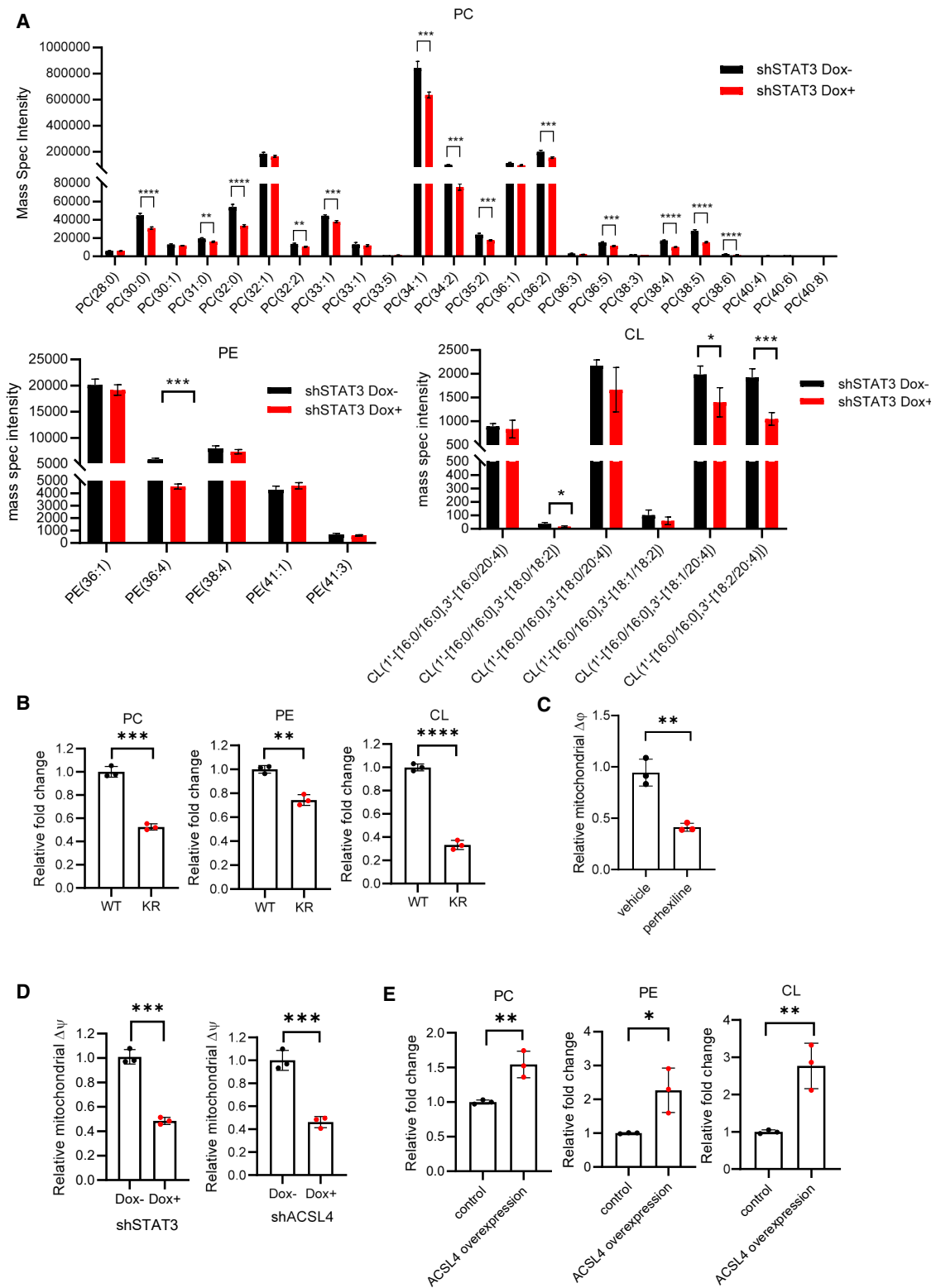


Figure 4. ACSL4-mediated phospholipid biogenesis upregulates mitochondrial $\Delta\psi$

(A) The lipid contents of PC, PE, and CL in MDA-MB-231-R cells with or without STAT3 gene knockdown (Dox+ or Dox-) were assessed and quantified by mass spectrometry.

(legend continued on next page)

quantified by using qPCR (Jasoliya et al., 2017; Redmann et al., 2018). We also assessed mitochondrial mass by MitoTracker Green staining and microscopy imaging (Doherty and Perl, 2017; Figures S4G and S4H).

To further demonstrate that the content of phospholipids in mitochondria is regulated by ACSL4, we ectopically expressed ACSL4 in parental MDA-MB-231 cells. TLC results showed the level of phospholipids in the mitochondria from ACSL4-expressing cells was significantly increased while mitochondrial mass remained similar (Figures 4E, S4I, and S4J).

Increasing mitochondrial membrane phospholipids resists paclitaxel-induced apoptosis

In TNBC tumor microenvironment, lipid droplets secreted from adipocytes containing fatty acids and phospholipid monolayer are shown to support tumorigenesis and chemoresistance (Cao, 2019; Clement et al., 2020; Wang et al., 2018). We found that adding exogenous LCFA (BSA-palmitate) to TNBC cells increased mitochondrial $\Delta\psi$ and attenuated paclitaxel-induced apoptosis (Figures 5A and S5A). Next, we further examined whether phospholipid content in mitochondrial membrane was changed upon BSA-palmitate or paclitaxel treatments. Level of PC, PE, and CL phospholipids was significantly increased by BSA-palmitate. Further, paclitaxel treatment decreased the level of PC, PE, and CL phospholipids, which was reversed by adding BSA-palmitate (Figure 5B). Cytochrome c is bound to the mitochondrial inner membrane by anionic phospholipids, mainly CL (Bergstrom et al., 2013; Gorbenko et al., 2006), and is released from mitochondria during the early stages of apoptosis (Liu et al., 1996; Ott et al., 2002). To determine whether increased phospholipids and mitochondrial $\Delta\psi$ would result in resistance to paclitaxel-induced apoptosis, cytochrome c release was examined by western blotting after cell fractionation and mitochondria enrichment (Figure 5C). Paclitaxel treatment significantly increased cytochrome c release from mitochondria to the cytoplasm. Importantly, BSA-palmitate treatment to increase phospholipids abrogated chemotherapy-induced cytochrome c release from mitochondria (Figure 5C), shown by apoptosis assay using annexin V staining (Figure 5A). To further provide direct evidence that phospholipids are important for protecting cells from chemotherapy-induced apoptosis, PC was first conjugated with BSA and subsequently added to cultured cells. Supplementing PC to elevate mitochondrial $\Delta\psi$ and PC phospholipid content significantly increased resistance to paclitaxel-induced cell death (Figures 5D and S5B).

We further investigated the extent to which mitochondrial depolarization, due to ACSL4 or STAT3 silencing, or FAO inhibi-

tion by perhexiline could induce TNBC tumor cell apoptosis. Annexin V binding and cleaved caspase 3 were significantly increased after STAT3 and ACSL4 knockdown and perhexiline treatment (Figure 5E). In addition, overexpression of ACSL4 in parental MDA-MB-231 cells partially rescued cell death induced by the chemotherapeutic reagent (Figures 5F and S5C).

To validate ACSL4 as a potential target to reverse chemoresistance via *de novo* phospholipid biosynthesis, we silenced ACSL4 and STAT3 in the chemoresistant tumor cells. Silencing ACSL4 or STAT3 effectively inhibited the growth of the chemoresistant TNBC tumors *in vivo* (Figures 6A–6C and S6A). Immunohistochemistry revealed that silencing ACSL4 or STAT3 decreased cell proliferation (Ki67) while increasing the level of cleaved caspase 3 (Figures 6D and 6E). Furthermore, phospholipid contents were significantly decreased in the mitochondrial membranes isolated from the tumor tissues with ACSL4 or STAT3 knockdown (Figures 6F and 6G), supporting that lowering mitochondrial membrane phospholipids through targeting ACSL4 or STAT3 inhibits TNBC tumor progression. CRISPR-Cas9-mediated ACSL4 or STAT3 gene perturbation (ACSL4 knockout [KO] and STAT3 KO) significantly inhibited tumor growth and proliferation, induced apoptosis, and decreased phospholipid contents in mitochondrial membrane in TNBC xenograft tumors (Figures S6B–S6G).

To further support our findings that inhibiting FAO or CPT1B expression reduced acetyl-STAT3 and acetyl-CoA (Figures 1A and 1B), we perturbed the CPT1B gene in MDA-MB-231-R cells by CRISPR-Cas9 approach. Like ACSL4 KO and STAT3 KO xenograft tumors, disrupting the CPT1B gene suppressed xenograft tumor growth and decreased the phospholipid contents in mitochondrial membrane prepared from the xenograft tumors (Figures S6H and S6I).

Ferroptosis is another type of programmed cell death linked to ACSL4 overexpression and accumulated lipid peroxides in cancer cells (Doll et al., 2017; Yuan et al., 2016). Lipid peroxides staining and flow cytometry analysis show that blocking ACSL4 or STAT3 did not induce noticeable ferroptosis (Figure S6J).

Targeting acetyl-STAT3 reduces TNBC tumor mitochondrial membrane phospholipids

Our data support a key role of acetyl-STAT3 in anti-apoptosis through upregulating phospholipids and mitochondrial $\Delta\psi$. We described in a recent report a cell-penetrating peptide that specifically targets acetyl-STAT3 at K685 (PS-acet.-)STAT3 peptide (Aftabzadeh et al., 2021). A control peptide, PO-acet.-STAT3 peptide, has the same amino acids and acetyl group modification

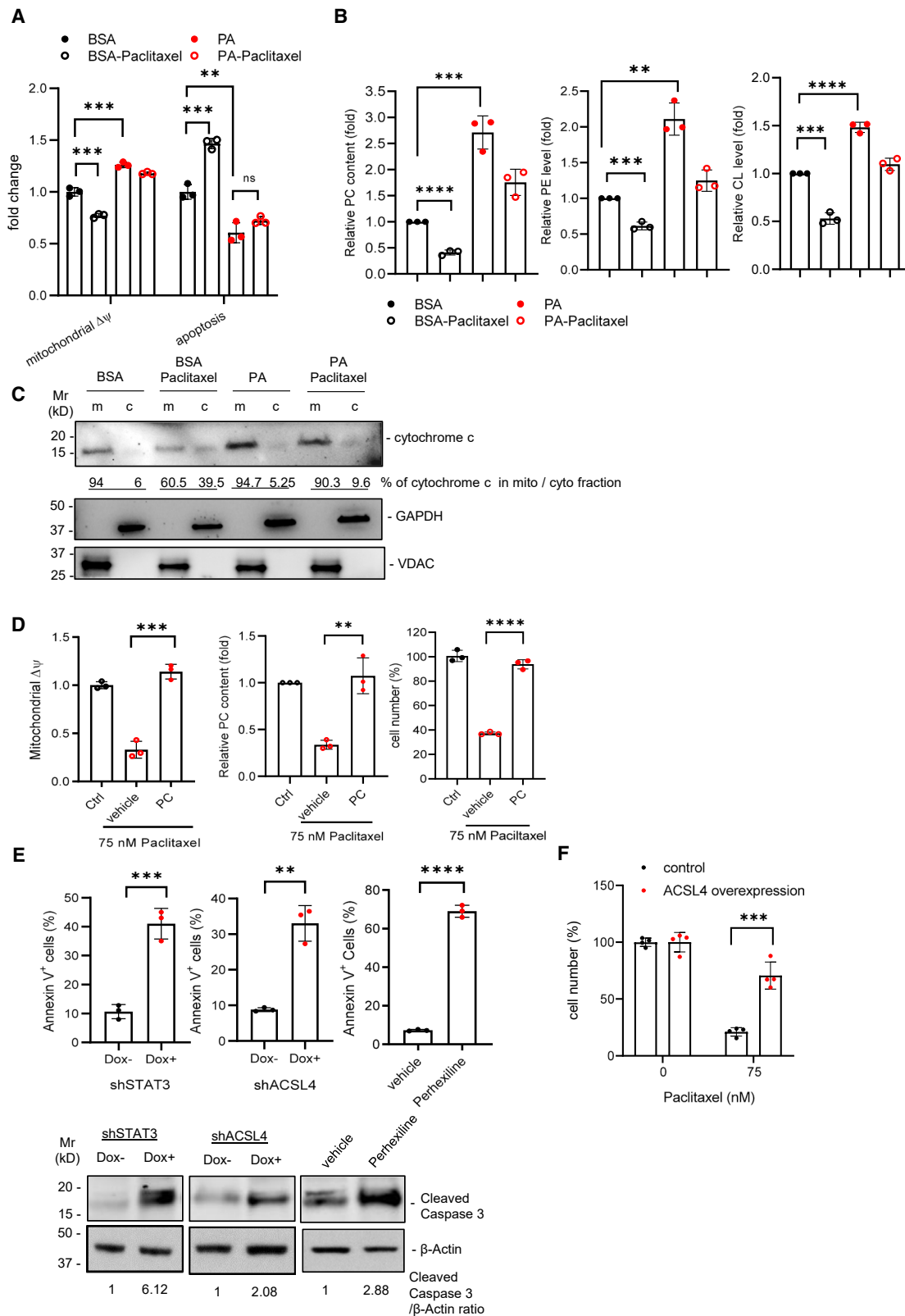
(B) Phospholipid content from cell membranes isolated from MDA-MB-231-R expressing WT or KR-STAT3 was analyzed by TLC. The quantification of phospholipid of PC, PE, and CL was performed by ImageJ software and shown in bar graphs.

(C) Mitochondrial $\Delta\psi$ in MDA-MB-231-R cells treated with either vehicle or perhexiline was assessed by JC1 staining and confocal microscopy. The graphs show the relative M.F.I. of JC1-red/JC1-green quantified by Zen software.

(D) The effects of STAT3 or ACSL4 knockdown (Dox+) on mitochondrial $\Delta\psi$ of MDA-MB-231-R cells were assessed by JC1 fluorescent staining and confocal microscopy.

(E) The levels of PC, PE, and CL in the mitochondrial membranes of MDA-MB-231 cells with or without ectopic expression of ACSL4 were measured by TLC and quantified by ImageJ software.

For all bar graphs, data are shown as mean \pm SD; n = 3; two-tailed, unpaired Student's t test. *p < 0.05; **p < 0.01; ***p < 0.005; ****p < 0.001. See also Figure S4 and Table S1D.



(legend on next page)

but no PS polymer backbone (Aftabzadeh et al., 2021). PS-acet.-STAT3 peptide efficiently penetrated into the primary tumor spheres (BBM3), but not the control PO-acet.-STAT3 peptide (Figure S7A). Moreover, blocking acetyl-STAT3 with PS-acet.-STAT3 peptide abrogated the elevated expression of ACSL4 and CPT1B in MDA-MB-231-R cells (Figure 7A). PS-acet.-STAT3 peptide also reduced FAO (Figure 7B), inhibited mitochondrial ATP generation (Figure 7C), depolarized mitochondrial $\Delta\psi$, and increased apoptosis in the chemoresistant TNBC cells (Figure 7D), which was abrogated by ACSL4 overexpression (Figure 7E).

We next assessed the anti-tumor effects of targeting acetyl-STAT3 using the PS-acet.-STAT3 peptide in MDA-MB-231-R orthotopic xenograft tumors. Systemic treatments with the PS-acet.-STAT3 peptide at a low concentration (1 mg/kg, intravenous [i.v.] injection) significantly induced potent anti-tumor effects and suppressed expression of ACSL4 and CPT1B (Figures 7F–7H). The volcano plot from differential expression of fatty acid metabolic genes indicated that the expression of ACSL4 and CPT1B was significantly suppressed by PS-acet.-STAT3 peptide treatment (Figure 7I). The finding is consistent with the assay from KR-STAT3-expressing cells (Figure 2B). Furthermore, immunohistochemistry staining of the tumor tissues showed that PS-acet.-STAT3 peptide treatment inhibited ACSL4 and Ki67 (Figure 7J) and decreased phospholipid contents in mitochondrial membranes derived from tumor tissues (Figure 7K). mtDNA was measured to confirm the reduction of phospholipid content was not due to changes in mitochondrial mass (Figure S7B).

DISCUSSION

FAO and lipid metabolism are essential for chemoresistance in cancers, including TNBC (Camarda et al., 2016; Casciano et al., 2020; Wright et al., 2017). However, these studies do not provide underlying mechanisms by which FAO promotes resistance to chemotherapy. Our current study demonstrates that extra acetyl-CoA generated by hyperactive FAO increases acetylation of STAT3, and acetyl-STAT3, in turn, upregulates ACSL/acyl-CoA to enhance phospholipid biosynthesis, thereby increasing mitochondrial membrane lipid content and potential to resist apoptosis.

It is generally known that acetyl-CoA does not efficiently penetrate cellular membranes. Our current study, through multiple approaches, indicates that acetyl-CoA derived mainly from FAO in the chemoresistant TNBC cells can be transported from mitochondria to cytosol. Our data further suggest that citrate acts as the intermediate. Although not necessarily expected, we show citrate level is elevated in the chemoresistant TNBC cells in which FAO is high. Our results further indicated that extracellular acetyl-CoA can penetrate the chemoresistant TNBC cells. It is possible the chemoresistant tumor cells may transport certain molecules, as some cancer cells (including TNBC) and immune cells can have distinct lipid and drug transporters (Chen et al., 2019b; Robey et al., 2018; Roderick and Cook, 2008; Song et al., 2020). Nevertheless, the mechanisms underlying acetyl-CoA membrane penetration in these tumor cells remain to be elucidated.

Our current work demonstrates the mechanism for STAT3 activation and acetylation by increased acetyl-CoA due to hyperactive FAO. This is supported by ¹⁴C-palmitic acid labeling experiment and by blocking or increasing FAO. Furthermore, we show that acetyl-STAT3 is elevated in both chemoresistant TNBC cell lines and metastatic patient tumor tissues compared with their non-resistant and primary counterparts. Although activation of STAT3 is frequently assessed by increased phosphorylation, our findings strongly support a critical role of acetylated STAT3 activity in cancer progression and resistance to therapy. We demonstrated the importance of STAT3 acetylation (K685) in chemoresistance through endogenous site-specific mutation at K685 as well as the PS-acet.-STAT3 peptide that targets STAT3 acetylation (K685), both *in vitro* and *in vivo*. These findings suggest that acetyl-STAT3 is an important target for overcoming chemoresistance in TNBC, in part by inhibiting ACSL4 and reducing mitochondrial membrane phospholipids.

Although FAO has been associated with cancer progression and chemoresistance, a high FAO activity level is expected to exhaust fatty acids, which may subsequently decrease *de novo* phospholipid biogenesis. We have identified ACSL4 as a STAT3 direct target gene. Our previous study indicated that breast tumor cells can take up LCFAs from surrounding adipocytes, mediated at least in part by CD36 (Wang et al., 2018). However, excessive fatty acid cell uptake results in lipotoxicity

Figure 5. FAO-STAT3 resists paclitaxel-induced apoptosis via increased phospholipids

(A) BSA or BSA-palmitate (BSA-PA) was added to cultured parental MDA-MB-231 cells before paclitaxel was added to induce apoptosis. Mitochondrial $\Delta\psi$ and apoptosis was assessed by JC1 staining and APC-annexin V staining. Fluorescence was detected by flow cytometry, and the M.F.I. was quantified by FlowJo software.

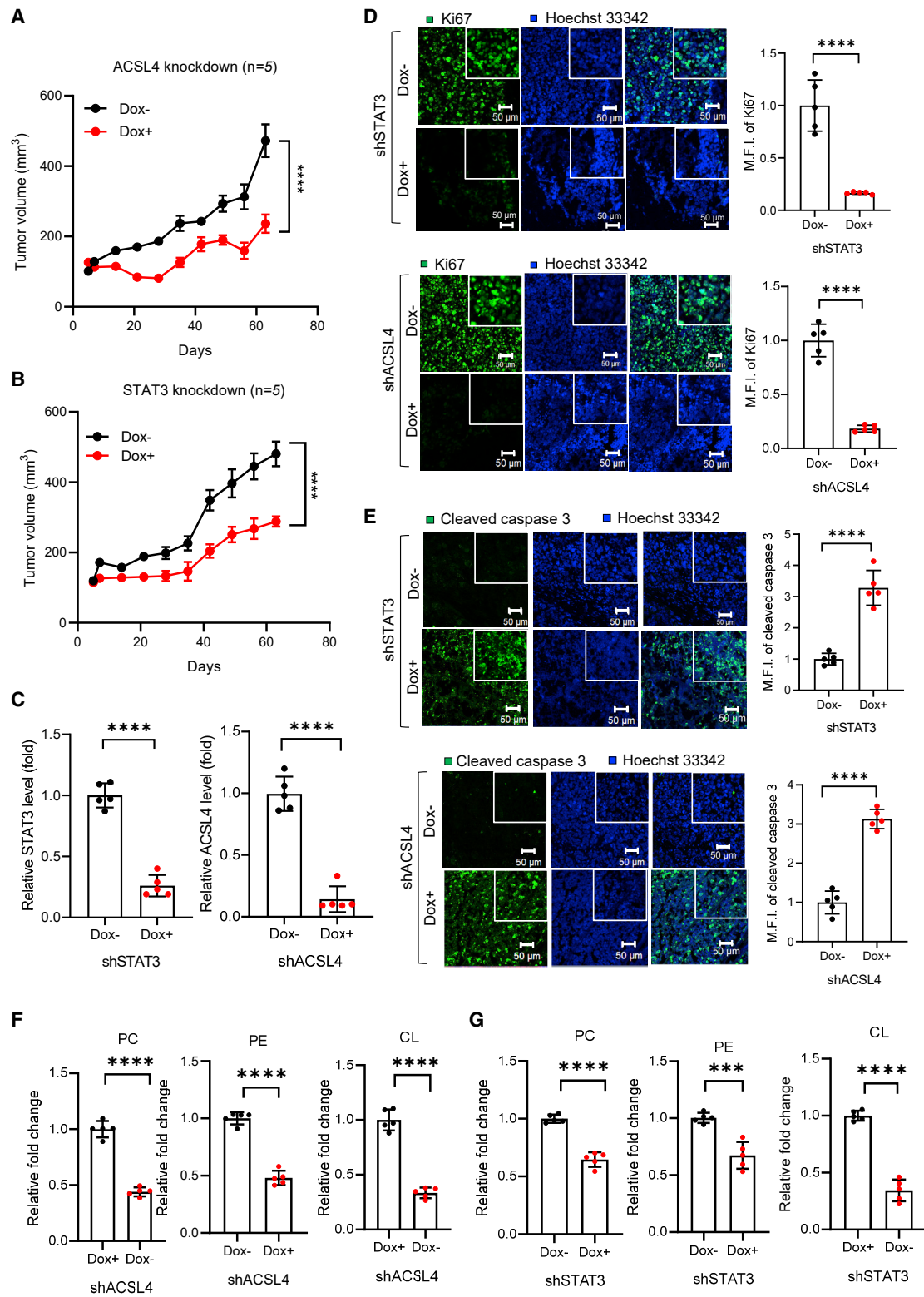
(B) The PC, PE, and CL phospholipid content in the mitochondria isolated from the cells described in (A) was analyzed by TLC and quantified by ImageJ software. The relative intensity of lipid spots was normalized with BSA treatment (normalize to 1) from each treatment.

(C) Cytochrome c released from mitochondria (m) to cytoplasm (c) in the samples described in (A) was examined by western blotting after cell fractionation. GAPDH and VDAC were detected as markers for cytoplasm and mitochondria fractions, respectively. The percentage of cytochrome c released from mitochondria to cytoplasm was quantified by band intensity of western blotting and ImageJ software.

(D) BSA (vehicle) or BSA-phospholipid PC (PC) was added to cultured MDA-MB-231-R cells before paclitaxel was added to induce apoptosis. Control cells were left untreated (Ctrl). Cell proliferation was measured by CyQUANT, and mitochondrial $\Delta\psi$ was monitored by JC1 staining. The PC phospholipid content in the mitochondria was analyzed by TLC and quantified by ImageJ software.

(E) Annexin-V/phosphatidylinositol (PI) staining (upper panels) and cleaved caspase 3 western blotting (lower panels) showed apoptosis in MDA-MB-231-R cells with or without ACSL4 and STAT3 knockdown or perhexiline treatment.

(F) ACSL4 overexpression in parental MDA-MB-231 cells restored cell survival upon paclitaxel treatment. Cell proliferation was determined by CyQUANT. n = 4. For the bar graphs in this figure, data are shown as mean \pm SD; n = 3 or 4, as indicated; two tailed and unpaired Student's t test. **p < 0.01; ***p < 0.005; ****p < 0.001. See also Figure S5 and Tables S1E, S2E, and S2F.



(legend on next page)

(Unger, 1995; Unger et al., 2010). The highly elevated ACSL expression in metastatic and therapy-resistant cancer cells therefore can lead to active fatty acid catabolism, which not only protects cells from lipotoxicity but also provides an extra energy source (ATP from FAO). ACSL supports ligation of CoA and fatty acids to form fatty acyl-CoAs, which is essential for phospholipid biogenesis and FAO. ACSL4 has also been reported to mediate metabolic channeling of fatty acids towards phosphatidylinositol synthesis in human hepatocytes (Kan et al., 2015) and phospholipid remodeling in obesity-associated adipocytes (Killion et al., 2018). Increased lipids and phospholipid biogenesis has been suggested to contribute to survival of cancer cells; however, little is known about the underlying mechanisms (Li et al., 2006; Maloberti et al., 2010; Padanad et al., 2016; Wu et al., 2015). Our data show that the acetyl-STAT3-ACSL pathway increases phospholipid biogenesis, mitochondrial $\Delta\psi$, leading to resistance to apoptosis.

In our previous study (Lee et al., 2012), acetyl-STAT3 was shown to suppress expression of TP53 in WT TP53-expressing cells to promote tumor progression. However, TP53 mutations or deletions are highly prevalent in TNBC tumors (Cancer Genome Atlas, 2012) and in TNBC cell lines we utilized in the experiments. It has also been shown that insulin-induced STAT3 acetylation in non-cancerous starved cells enables STAT3 mitochondrial translocation, whereby STAT3 associates with pyruvate dehydrogenase complex E1, leading to elevated mitochondrial $\Delta\psi$ and ATP synthesis (Xu et al., 2016). These findings suggest that acetylated STAT3 may promote mitochondrial $\Delta\psi$ via additional mechanisms. Nevertheless, in the chemoresistant TNBC cells, an association of acetyl-STAT3 with pyruvate metabolism was not detected (data not shown).

In conclusion, our study has unraveled a mechanism by which elevated FAO promotes anti-apoptosis in chemoresistant TNBC cells. We further demonstrated that acetyl-STAT3 and ACSL-4, in addition to FAO/CPT1, are promising targets to overcome chemoresistance in TNBC.

Limitations of the study

To demonstrate how active FAO increases the level of acetyl-CoA in cytosolic pool, we employed colorimetric assays to measure the abundance of citrate, pyruvate, or acetyl-CoA in parental and chemoresistant TNBC cells. Although commonly used, the colorimetric assays may only measure the level of metabolites in cells, not the production rate.

Ideally, gel electrophoresis and autoradiography is the methodology of choice to show the substrate specificity of ^{14}C -palmitic acid labeling assay. However, we encountered some tech-

nical challenges due to relatively high radioisotope background on radiographic films after long exposure. Therefore, scintillation counting was used for quantifying the level of ^{14}C -STAT3 from ^{14}C -palmitic acid labeling assay in this study.

It is generally accepted that acetyl-CoA does not efficiently penetrate cells. However, we have previously shown that chemoresistant TNBC cells could uptake ^{14}C or ^3H -acetyl-CoA and adding acetyl-CoA to cultured chemoresistant TNBC cells increased tumor cell survival (Wang et al., 2018). In the current study, we also show that adding acetyl-CoA promoted the level of acetyl-STAT3 in multiple cell lines (Figures S1B and S1C). These findings may be limited to certain subtypes of cells, in our case, chemoresistant TNBC cells. Future studies are required to identify the mechanism(s) underlying acetyl-CoA cell penetration.

STAR★METHODS

Detailed methods are provided in the online version of this paper and include the following:

- KEY RESOURCES TABLE
- RESOURCE AVAILABILITY
 - Lead contact
 - Materials availability
 - Data and code availability
- EXPERIMENTAL MODEL AND SUBJECT DETAILS
 - Mice
 - Cell lines
 - Patient breast tumor specimens
- METHOD DETAILS
 - Cell culture/splenic CD8⁺ T cell isolation
 - Plasmids and siRNAs
 - Mitochondrial DNA quantification
 - *In vivo* experiments
 - Immunoblotting and immunoprecipitation
 - Fluorescent microscopy imaging
 - Cell proliferation assay
 - Acetyl-CoA assay
 - Citrate fluorometric assay
 - Pyruvate fluorometric assay
 - ATP-based bioluminescence assay
 - Quantitative real-time PCR (qPCR)
 - Microarray analysis
 - Chromatin immunoprecipitation (ChIP) assay
 - ^{14}C -palmitic acid labeling
 - Thin-layer chromatography (TLC)
 - Mitochondria preparation

Figure 6. Silencing ACSL4 or STAT3 reduces mitochondrial membrane lipids and chemoresistant TNBC tumor growth

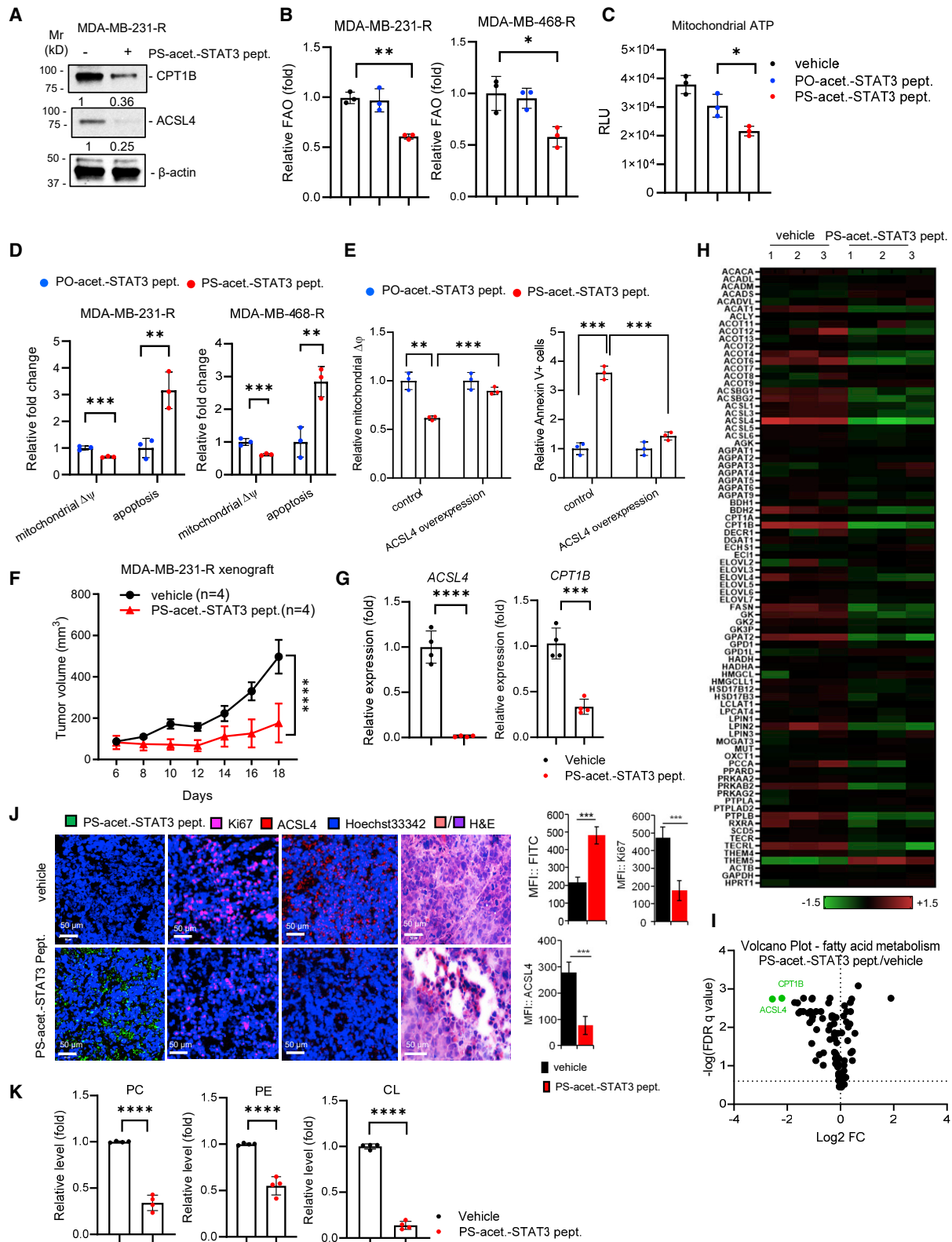
(A and B) MDA-MB-231-R cells were orthotopically implanted in the mammary fat pad of female non-obese diabetic (NOD)/severe combined immunodeficiency (SCID)-interleukin (IL)-2R γ c-null (NSG) mice. Doxycycline was supplied to induce shRNA targeting ACSL4 (A) or STAT3 (B) until the end time point. Tumor growth kinetic was measured by tumor size, and the data are shown as mean \pm SEM; n = 5 mice/group; two-way ANOVA; ****p < 0.001.

(C) The protein level of STAT3 and ACSL4 in the individual xenograft tumors was assessed by western blotting.

(D and E) Immunohistochemistry of tumor sections from (A) and (B). The levels of Ki67 (D) and cleaved caspase 3 (E) were visualized by IHC, and M.F.I. was quantified and shown in bar graphs (n = 5, right panel). Hoechst 33342 was used for nuclear counter-staining. The representative images of five samples are shown. Scale bars, 50 μm .

(F and G) The levels of PC, PE, and CL in the mitochondrial membranes isolated from the individual tumors with or without ACSL4 (F) or STAT3 gene knockdown (G) were analyzed by TLC and quantified by ImageJ software.

Data shown in (C)–(G) are mean \pm SD; n = 5 tumor samples; two tailed and unpaired Student's t test. ***p < 0.005; ****p < 0.001. See also Figure S6 and Table S1F.



(legend on next page)

- JC-1 staining of mitochondrial $\Delta\psi$
- MitoTracker green labeling
- Fatty acid oxidation assay
- Ferroptosis assay
- Annexin V/PI apoptosis assay
- Lipid analysis-Mass spectrometry
- Oligopeptide structure and synthesis
- Peptide penetration

● **QUANTIFICATION AND STATISTICAL ANALYSIS**

SUPPLEMENTAL INFORMATION

Supplemental information can be found online at <https://doi.org/10.1016/j.celrep.2022.110870>.

ACKNOWLEDGMENTS

We thank Dr. Antons Martincuks for generating the graphical abstract. Graphical abstract was created with [BioRender.com](https://www.biorender.com). We appreciate the technical support from Pathology-Solid Tumor, Integrative Genomic, Analytical Cytometry, and Light Microscopy Core facilities at the Beckman Research Institute at City of Hope. We also thank the staff members at the Animal Research Core Facility (including Animal Tumor Models Program) at City of Hope. This work was supported by institutional funds and by National Cancer Institute R01CA247368. Research reported in this publication was also supported under grant number National Cancer Institute P30CA033572. The content is solely the responsibility of the authors and does not necessarily represent the official views of the NIH.

AUTHOR CONTRIBUTIONS

Conceptualization, Y.-J.L. and H.Y.; methodology and investigation, Y.-J.L., J.F.F. (metabolomic analysis), M.A., S.C.T. (metabolomic analysis), Q.Z., C.Z., and H.Y.; writing & editing, Y.-J.L. and H.Y.; resources, Y.Y. and S.H.; funding acquisition and supervision, H.Y. and D.A.

DECLARATION OF INTERESTS

H.Y. has patent applications related to cell-penetrating peptide. Y.-J.L. and H.Y. serve as consultants at Inova BioTherapeutics, Inc.

Received: March 18, 2021
Revised: March 16, 2022
Accepted: May 4, 2022
Published: May 31, 2022; corrected online June 17, 2022

REFERENCES

Aftabzadeh, M., Li, Y.J., Zhao, Q., Zhang, C., Ambaye, N., Song, J., Nagao, T., Lahtz, C., Fakhri, M., Ann, D.K., et al. (2021). Potent antitumor effects of cell-penetrating peptides targeting STAT3 axis. *JCI Insight* 6, e136176. <https://doi.org/10.1172/jci.insight.136176>.

Aicheler, F., Li, J., Hoene, M., Lehmann, R., Xu, G., and Kohlbacher, O. (2015). Retention time prediction improves identification in nontargeted lipidomics approaches. *Anal. Chem.* 87, 7698–7704. <https://doi.org/10.1021/acs.analchem.5b01139>.

Aloia, A., Mullhaupt, D., Chabbert, C.D., Eberhart, T., Flückiger-Mangual, S., Vukolic, A., Eichhoff, O.M., Irmisch, A., Alexander, L.T., Scibona, E., et al. (2019). A fatty acid oxidation-dependent metabolic shift regulates the adaptation of BRAF-mutated melanoma to MAPK inhibitors. *Clin. Cancer Res.* 25, 6852–6867. <https://doi.org/10.1158/1078-0432.CCR-19-0253>.

Bergstrom, C.L., Beales, P.A., Lv, Y., Vanderlick, T.K., and Groves, J.T. (2013). Cytochrome c causes pore formation in cardiolipin-containing membranes. *Proc. Natl. Acad. Sci. U S A* 110, 6269–6274. <https://doi.org/10.1073/pnas.1303819110>.

Cai, L., Sutter, B.M., Li, B., and Tu, B.P. (2011). Acetyl-CoA induces cell growth and proliferation by promoting the acetylation of histones at growth genes. *Mol. Cell* 42, 426–437. <https://doi.org/10.1016/j.molcel.2011.05.004>.

Camarda, R., Zhou, A.Y., Kohnz, R.A., Balakrishnan, S., Mahieu, C., Anderton, B., Eyob, H., Kajimura, S., Tward, A., Krings, G., et al. (2016). Inhibition of fatty acid oxidation as a therapy for MYC-overexpressing triple-negative breast cancer. *Nat. Med.* 22, 427–432. <https://doi.org/10.1038/nm.4055>.

Cancer Genome Atlas, N. (2012). Comprehensive molecular portraits of human breast tumours. *Nature* 490, 61–70. <https://doi.org/10.1038/nature11412>.

Cao, Y. (2019). Adipocyte and lipid metabolism in cancer drug resistance. *J. Clin. Invest.* 129, 3006–3017. <https://doi.org/10.1172/JCI127201>.

Carey, M.F., Peterson, C.L., and Smale, S.T. (2009). Chromatin immunoprecipitation (ChIP). *Cold Spring Harb Protoc.* 2009, pdb prot5279. <https://doi.org/10.1101/pdb.prot5279>.

Figure 7. Targeting acetyl-STAT3 reduces mitochondrial membrane lipids and induces tumor cell apoptosis *in vitro* and *in vivo*

(A) PS-acet.-STAT3 pept. treatment in MDA-MB-231-R cells reduced ACSL4 and CPT1B upregulation. The protein levels of CPT1B or ACSL4 were assessed by western blotting.

(B) PS-acet.-STAT3 pept. treatment reduced FAO in two chemoresistant TNBC cell lines. Data shown are mean \pm SD; n = 3; one-way ANOVA; *p < 0.05; **p < 0.01.

(C) PS-acet.-STAT3 pept. treatment in MDA-MB-231-R cells reduced mitochondrial ATP level. Mitochondria were isolated from the cells receiving indicated treatments before performing ATP-based bioluminescence assay. RLU, relative light unit.

(D) PS-acet.-STAT3 pept. treatment decreased mitochondrial $\Delta\psi$ and increased apoptosis in two chemoresistant TNBC cell lines. Mitochondrial $\Delta\psi$ and apoptosis were examined by flow cytometry as described above.

(E) ACSL4 overexpression in parental MDA-MB-231 cells restored the loss of mitochondrial $\Delta\psi$ and apoptosis induced by PS-acet.-STAT3 pept. treatment. Mitochondrial $\Delta\psi$ and apoptosis were assessed as described above.

(F) Growth kinetics of MDA-MB-231-R xenograft tumors upon PS-acet.-STAT3 pept. treatment. The tumor-bearing mice were given i.v. treatments, as indicated. n = 4 mice/group. The data shown are mean \pm SEM; two-way ANOVA; ****p < 0.0001.

(G) qPCR shows gene expression of *ACSL4* or *CPT1B* in the TNBC tumor tissues from (F).

(H) The heatmap showing fatty acid metabolic genes differentially expressed in the xenograft tumors treated shown in (F). RNA samples from each group were pooled to perform microarray analysis. The data (n = 3 independent assays) are shown by the log₂ fold changes. –1.5 to +1.5, green-to-red (color intensity gradient).

(I) Volcano plot depicting differentially expressed genes described in (H), showing the significant downregulation of *ACSL4* and *CPT1B* after TNBC tumors treated with PS-acet.-STAT3 pept. y axis denotes –log₁₀ FDR q values, while x axis shows log₂ fold change values. Volcano plot was generated using GraphPad Prism.

(J) Fluorescent immunohistochemistry of tumor section from (F). The level of PS-acet.-STAT3 pept., Ki67, or ACSL4 was assessed by IHC, and the M.F.I. was quantified and shown in bar graphs. Scale bars, 50 μ m.

(K) The levels of PC, PE, and CL in the mitochondrial membranes isolated from MDA-MB-231-R xenografts as shown in (F) were analyzed by TLC and quantified by ImageJ software.

Data shown in (B)–(E) are mean \pm SD; n = 3 biological replicates; data shown in (G), (J), and (K) are mean \pm SD; n = 4 tumor samples; two-tailed and unpaired Student's t test. *p < 0.05; **p < 0.01; ***p < 0.005; ****p < 0.0001. See also [Figure S7](#) and [Table S1G](#).

- Carracedo, A., Cantley, L.C., and Pandolfi, P.P. (2013). Cancer metabolism: fatty acid oxidation in the limelight. *Nat. Rev. Cancer* 13, 227–232. <https://doi.org/10.1038/nrc3483>.
- Casciano, J.C., Perry, C., Cohen-Nowak, A.J., Miller, K.D., Vande Voorde, J., Zhang, Q.F., Chalmers, S., Sandison, M.E., Liu, Q., Hedley, A., et al. (2020). MYC regulates fatty acid metabolism through a multigenic program in claudin-low triple negative breast cancer. *Br. J. Cancer* 122, 868–884. <https://doi.org/10.1038/s41416-019-0711-3>.
- Chen, R.R., Yung, M.M.H., Xuan, Y., Zhan, S., Leung, L.L., Liang, R.R., Leung, T.H.Y., Yang, H., Xu, D., Sharma, R., et al. (2019a). Targeting of lipid metabolism with a metabolic inhibitor cocktail eradicates peritoneal metastases in ovarian cancer cells. *Commun. Biol.* 2, 281. <https://doi.org/10.1038/s42003-019-0508-1>.
- Chen, Y., Fan, Z.M., Yang, Y., and Gu, C.Y. (2019b). Iron metabolism and its contribution to cancer (Review). *Int. J. Oncol.* 54, 1143–1154. <https://doi.org/10.3892/ijo.2019.4720>.
- Cheng, S., Wang, G., Wang, Y., Cai, L., Qian, K., Ju, L., Liu, X., Xiao, Y., and Wang, X. (2019). Fatty acid oxidation inhibitor etomoxir suppresses tumor progression and induces cell cycle arrest via PPAR γ -mediated pathway in bladder cancer. *Clin. Sci.* 133, 1745–1758. <https://doi.org/10.1042/CS20190587>.
- Clement, E., Lazar, I., Attane, C., Carrie, L., Dauvillier, S., Ducoux-Petit, M., Esteve, D., Menneteau, T., Moutahir, M., Le Gonidec, S., et al. (2020). Adipocyte extracellular vesicles carry enzymes and fatty acids that stimulate mitochondrial metabolism and remodeling in tumor cells. *Embo J.* 39, e102525. <https://doi.org/10.15252/embo.2019102525>.
- Comerford, S.A., Huang, Z., Du, X., Wang, Y., Cai, L., Witkiewicz, A.K., Walters, H., Tantawy, M.N., Fu, A., Manning, H.C., et al. (2014). Acetate dependence of tumors. *Cell* 159, 1591–1602. <https://doi.org/10.1016/j.cell.2014.11.020>.
- Crimi, M., and Esposti, M.D. (2011). Apoptosis-induced changes in mitochondrial lipids. *BBA Mol. Cell. Res.* 1813, 551–557. <https://doi.org/10.1016/j.bbamcr.2010.09.014>.
- Daum, G. (1985). Lipids of mitochondria. *Biochim. Biophys. Acta* 822, 1–42. [https://doi.org/10.1016/0304-4157\(85\)90002-4](https://doi.org/10.1016/0304-4157(85)90002-4).
- Dijk, S.N., Protasoni, M., Elpidorou, M., Kroon, A.M., and Taanman, J.W. (2020). Mitochondria as target to inhibit proliferation and induce apoptosis of cancer cells: the effects of doxycycline and gemcitabine. *Sci. Rep.* 10, 4363. <https://doi.org/10.1038/s41598-020-61381-9>.
- Doherty, E., and Perl, A. (2017). Measurement of mitochondrial mass by flow cytometry during oxidative stress. *React. Oxyg Species* 4, 275–283. <https://doi.org/10.20455/ros.2017.839>.
- Doll, S., Proneth, B., Tyurina, Y.Y., Panzilius, E., Kobayashi, S., Ingold, I., Irmeler, M., Beckers, J., Aichler, M., Walch, A., et al. (2017). ACSL4 dictates ferroptosis sensitivity by shaping cellular lipid composition. *Nat. Chem. Biol.* 13, 91–98. <https://doi.org/10.1038/nchembio.2239>.
- Duman, C., Yaqubi, K., Hoffmann, A., Acikgoz, A.A., Korshunov, A., Bendszus, M., Herold-Mende, C., Liu, H.K., and Alfonso, J. (2019). Acyl-CoA-binding protein drives glioblastoma tumorigenesis by sustaining fatty acid oxidation. *Cell Metab.* 30, 274–289.e5. <https://doi.org/10.1016/j.cmet.2019.04.004>.
- Edmunds, L.R., Sharma, L., Kang, A., Lu, J., Vockley, J., Basu, S., Uppala, R., Goetzman, E.S., Beck, M.E., Scott, D., and Prochownik, E.V. (2014). c-Myc programs fatty acid metabolism and dictates acetyl-CoA abundance and fate. *J. Biol. Chem.* 289, 25382–25392. <https://doi.org/10.1074/jbc.M114.580662>.
- Fabbri, F., Carloni, S., Briigliadori, G., Zoli, W., Lapalombella, R., and Marini, M. (2006). Sequential events of apoptosis involving docetaxel, a microtubule-interfering agent: a cytometric study. *BMC Cell Biol.* 7, 6. <https://doi.org/10.1186/1471-2121-7-6>.
- Gohil, V.M., and Greenberg, M.L. (2009). Mitochondrial membrane biogenesis: phospholipids and proteins go hand in hand. *J. Cell Biol.* 184, 469–472. <https://doi.org/10.1083/jcb.200901127>.
- Garbenko, G.P., Molotkovsky, J.G., and Kinnunen, P.K. (2006). Cytochrome C interaction with cardiolipin/phosphatidylcholine model membranes: effect of cardiolipin protonation. *Biophys. J.* 90, 4093–4103. <https://doi.org/10.1529/biophysj.105.080150>.
- Hattingen, E., Bahr, O., Rieger, J., Blasel, S., Steinbach, J., and Pilatus, U. (2013). Phospholipid metabolites in recurrent glioblastoma: in vivo markers detect different tumor phenotypes before and under antiangiogenic therapy. *PLoS One* 8, e56439. <https://doi.org/10.1371/journal.pone.0056439>.
- He, W., Liang, B., Wang, C., Li, S., Zhao, Y., Huang, Q., Liu, Z., Yao, Z., Wu, Q., Liao, W., et al. (2019). MSC-regulated lncRNA MACC1-AS1 promotes stemness and chemoresistance through fatty acid oxidation in gastric cancer. *Oncogene* 38, 4637–4654. <https://doi.org/10.1038/s41388-019-0747-0>.
- Houston, R., Sekine, S., Calderon, M.J., Seifuddin, F., Wang, G.H., Kawagishi, H., Malide, D.A., Li, Y.S., Gucek, M., Pirooznia, M., Nelson, A.J., Stokes, M.P., Stewart-Ornstein, J., Mullett, S.J., Wendell, S.G., Watkins, S.C., Finkel, T., and Sekine, Y. (2020). Acetylation-mediated remodeling of the nucleolus regulates cellular acetyl-CoA responses. *PLoS Biol.* 18, e3000981. <https://doi.org/10.1371/journal.pbio.3000981>.
- Houten, S.M., and Wanders, R.J.A. (2010). A general introduction to the biochemistry of mitochondrial fatty acid beta-oxidation. *J. Inher. Metab. Dis.* 33, 469–477. <https://doi.org/10.1007/s10545-010-9061-2>.
- Ishikawa, S., Tateya, I., Hayasaka, T., Masaki, N., Takizawa, Y., Ohno, S., Kojima, T., Kitani, Y., Kitamura, M., Hirano, S., et al. (2012). Increased expression of phosphatidylcholine (16:0/18:1) and (16:0/18:2) in thyroid papillary cancer. *PLoS One* 7, e48873. <https://doi.org/10.1371/journal.pone.0048873>.
- Jasoliya, M.J., McMackin, M.Z., Henderson, C.K., Perlman, S.L., and Cortopassi, G.A. (2017). Frataxin deficiency impairs mitochondrial biogenesis in cells, mice and humans. *Hum. Mol. Genet.* 26, 2627–2633. <https://doi.org/10.1093/hmg/ddx141>.
- Kan, C.F.K., Singh, A.B., Dong, B., Shende, V.R., and Liu, J. (2015). PPAR δ activation induces hepatic long-chain acyl-CoA synthetase 4 expression in vivo and in vitro. *Biochim. Biophys. Acta* 1851, 577–587. <https://doi.org/10.1016/j.bbali.2015.01.008>.
- Khan, A., Fornes, O., Stigliani, A., Gheorghe, M., Castro-Mondragon, J.A., van der Lee, R., Bessy, A., Cheneby, J., Kulkarni, S.R., Tan, G., et al. (2018). Jaspar 2018: update of the open-access database of transcription factor binding profiles and its web framework. *Nucleic Acids Res.* 46, D1284. <https://doi.org/10.1093/nar/gkx1188>.
- Kidd, J.F., Pilkington, M.F., Schell, M.J., Fogarty, K.E., Skepper, J.N., Taylor, C.W., and Thorn, P. (2002). Paclitaxel affects cytosolic calcium signals by opening the mitochondrial permeability transition pore. *J. Biol. Chem.* 277, 6504–6510. <https://doi.org/10.1074/jbc.M106802200>.
- Killion, E.A., Reeves, A.R., El Azzouny, M.A., Yan, Q.W., Surujon, D., Griffin, J.D., Bowman, T.A., Wang, C., Matthan, N.R., Klett, E.L., et al. (2018). A role for long-chain acyl-CoA synthetase-4 (ACSL4) in diet-induced phospholipid remodeling and obesity-associated adipocyte dysfunction. *Mol. Metab.* 9, 43–56. <https://doi.org/10.1016/j.molmet.2018.01.012>.
- Lee, H., Zhang, P., Herrmann, A., Yang, C.M., Xin, H., Wang, Z.H., Hoon, D.S.B., Forman, S.J., Jove, R., Riggs, A.D., and Yu, H. (2012). Acetylated STAT3 is crucial for methylation of tumor-suppressor gene promoters and inhibition by resveratrol results in demethylation. *Proc. Natl. Acad. Sci. U S A* 109, 7765–7769. <https://doi.org/10.1073/pnas.1205132109>.
- Li, L.O., Mashek, D.G., An, J., Doughman, S.D., Newgard, C.B., and Coleman, R.A. (2006). Overexpression of rat long chain acyl-CoA synthetase 1 alters fatty acid metabolism in rat primary hepatocytes. *J. Biol. Chem.* 281, 37246–37255. <https://doi.org/10.1074/jbc.M604427200>.
- Liu, X., Kim, C.N., Yang, J., Jemmerson, R., and Wang, X. (1996). Induction of apoptotic program in cell-free extracts: requirement for dATP and cytochrome c. *Cell* 86, 147–157. [https://doi.org/10.1016/s0092-8674\(00\)80085-9](https://doi.org/10.1016/s0092-8674(00)80085-9).
- Maloberti, P.M., Duarte, A.B., Orlando, U.D., Pasqualini, M.E., Solano, A.R., Lopez-Otin, C., and Podesta, E.J. (2010). Functional interaction between acyl-CoA synthetase 4, lipooxygenases and cyclooxygenase-2 in the aggressive phenotype of breast cancer cells. *PLoS One* 5, e15540. <https://doi.org/10.1371/journal.pone.0015540>.

- Martinez, A.M., Kim, A., and Yang, W.S. (2020). Detection of ferroptosis by BODIPYTM 581/591 C11. *Methods Mol. Biol.* 2108, 125–130. https://doi.org/10.1007/978-1-0716-0247-8_11.
- Mejia, E.M., and Hatch, G.M. (2015). Erratum to: mitochondrial phospholipids: role in mitochondrial function. *J. Bioenerg. Biomembr.* 47, 279–280. <https://doi.org/10.1007/s10863-015-9607-y>.
- Neman, J., Termini, J., Wilczynski, S., Vaidehi, N., Choy, C., Kowolik, C.M., Li, H., Hambrecht, A.C., Roberts, E., and Jandial, R. (2014). Human breast cancer metastases to the brain display GABAergic properties in the neural niche. *Proc. Natl. Acad. Sci. U S A* 111, 984–989. <https://doi.org/10.1073/pnas.1322098111>.
- Osman, C., Voelker, D.R., and Langer, T. (2011). Making heads or tails of phospholipids in mitochondria. *J. Cell Biol.* 192, 7–16. <https://doi.org/10.1083/jcb.201006159>.
- Ott, M., Robertson, J.D., Gogvadze, V., Zhivotovsky, B., and Orrenius, S. (2002). Cytochrome c release from mitochondria proceeds by a two-step process. *Proc. Natl. Acad. Sci. U S A* 99, 1259–1263. <https://doi.org/10.1073/pnas.241655498>.
- Padanad, M.S., Konstantinidou, G., Venkateswaran, N., Melegari, M., Rindhe, S., Mitsche, M., Yang, C.D., Batten, K., Huffman, K.E., Liu, J.W., et al. (2016). Fatty acid oxidation mediated by acyl-CoA synthetase long chain 3 is required for mutant KRAS lung tumorigenesis. *Cell Rep.* 16, 1614–1628. <https://doi.org/10.1016/j.celrep.2016.07.009>.
- Paradies, G., Paradies, V., De Benedictis, V., Ruggiero, F.M., and Petrosillo, G. (2014). Functional role of cardiolipin in mitochondrial bioenergetics. *Bba-Bioenergetics* 1837, 408–417. <https://doi.org/10.1016/j.bbabi.2013.10.006>.
- Pavlova, N.N., and Thompson, C.B. (2016). The emerging hallmarks of cancer metabolism. *Cell Metab.* 23, 27–47. <https://doi.org/10.1016/j.cmet.2015.12.006>.
- Perelman, A., Wachtel, C., Cohen, M., Haupt, S., Shapiro, H., and Tzur, A. (2012). JC-1: alternative excitation wavelengths facilitate mitochondrial membrane potential cytometry. *Cell Death Dis.* 3, e430. <https://doi.org/10.1038/cddis.2012.171>.
- Pougovkina, O., te Brinke, H., Ofman, R., van Cruchten, A.G., Kulik, W., Wanders, R.J., Houten, S.M., and de Boer, V.C. (2014). Mitochondrial protein acetylation is driven by acetyl-CoA from fatty acid oxidation. *Hum. Mol. Genet.* 23, 3513–3522. <https://doi.org/10.1093/hmg/ddu059>.
- Qu, Q., Zeng, F., Liu, X., Wang, Q.J., and Deng, F. (2016). Fatty acid oxidation and carnitine palmitoyltransferase I: emerging therapeutic targets in cancer. *Cell Death Dis* 7, e2226. <https://doi.org/10.1038/cddis.2016.132>.
- Redmann, M., Benavides, G.A., Wani, W.Y., Berryhill, T.F., Ouyang, X.S., Johnson, M.S., Ravi, S., Mitra, K., Barnes, S., Darley-Usmar, V.M., and Zhang, J. (2018). Methods for assessing mitochondrial quality control mechanisms and cellular consequences in cell culture. *Redox Biol.* 17, 59–69. <https://doi.org/10.1016/j.redox.2018.04.005>.
- Rhodes, D.R., Yu, J., Shanker, K., Deshpande, N., Varambally, R., Ghosh, D., Barrette, T., Pander, A., and Chinnaiyan, A.M. (2004). ONCOMINE: a cancer microarray database and integrated data-mining platform. *Neoplasia* 6, 1–6. [https://doi.org/10.1016/s1476-5586\(04\)80047-2](https://doi.org/10.1016/s1476-5586(04)80047-2).
- Robey, R.W., Pluchino, K.M., Hall, M.D., Fojo, A.T., Bates, S.E., and Gottesman, M.M. (2018). Revisiting the role of ABC transporters in multidrug-resistant cancer. *Nat. Rev. Cancer* 18, 452–464. <https://doi.org/10.1038/s41568-018-0005-8>.
- Roderick, H.L., and Cook, S.J. (2008). Ca²⁺ signalling checkpoints in cancer: remodelling Ca²⁺ for cancer cell proliferation and survival. *Nat. Rev. Cancer* 8, 361–375. <https://doi.org/10.1038/nrc2374>.
- Schenkel, L.C., and Bakovic, M. (2014). Formation and regulation of mitochondrial membranes. *Int. J. Cell. Biol.* 2014, 709828. <https://doi.org/10.1155/2014/709828>.
- Shi, L., and Tu, B.P. (2015). Acetyl-CoA and the regulation of metabolism: mechanisms and consequences. *Curr. Opin. Cell Biol.* 33, 125–131. <https://doi.org/10.1016/j.ceb.2015.02.003>.
- Sivandzade, F., Bhalerao, A., and Cucullo, L. (2019). Analysis of the mitochondrial membrane potential using the cationic JC-1 dye as a sensitive fluorescent probe. *Bio Protoc.* 9, e3128. <https://doi.org/10.21769/BioProtoc.3128>.
- Smiley, S.T., Reers, M., Mottola-Hartshorn, C., Lin, M., Chen, A., Smith, T.W., Steele, G.D., Jr., and Chen, L.B. (1991). Intracellular heterogeneity in mitochondrial membrane potentials revealed by a J-aggregate-forming lipophilic cation JC-1. *Proc. Natl. Acad. Sci. U S A* 88, 3671–3675. <https://doi.org/10.1073/pnas.88.9.3671>.
- Song, W.X., Li, D.Y., Tao, L., Luo, Q., and Chen, L.G. (2020). Solute carrier transporters: the metabolic gatekeepers of immune cells. *Acta Pharmacol. Sin B* 10, 61–78. <https://doi.org/10.1016/j.apsb.2019.12.006>.
- Tatsuta, T., Scharwey, M., and Langer, T. (2014). Mitochondrial lipid trafficking. *Trends Cell Biol.* 24, 44–52. <https://doi.org/10.1016/j.tcb.2013.07.011>.
- Unger, R.H. (1995). Lipotoxicity in the pathogenesis of obesity-dependent niddm - genetic and clinical implications. *Diabetes* 44, 863–870. <https://doi.org/10.2337/diabetes.44.8.863>.
- Unger, R.H., Clark, G.O., Scherer, P.E., and Orci, L. (2010). Lipid homeostasis, lipotoxicity and the metabolic syndrome. *Bba-mol Cell Biol. L* 1801, 209–214. <https://doi.org/10.1016/j.bbali.2009.10.006>.
- van der Veen, J.N., Kennelly, J.P., Wan, S., Vance, J.E., Vance, D.E., and Jacobs, R.L. (2017). The critical role of phosphatidylcholine and phosphatidylethanolamine metabolism in health and disease. *Bba-Biomembranes* 1859, 1558–1572. <https://doi.org/10.1016/j.bbame.2017.04.006>.
- Wang, T., Fahrman, J.F., Lee, H., Li, Y.J., Tripathi, S.C., Yue, C., Zhang, C., Lifshitz, V., Song, J., Yuan, Y., et al. (2018). JAK/STAT3-Regulated fatty acid beta-oxidation is critical for breast cancer stem cell self-renewal and chemoresistance. *Cell Metab.* 27, 136–150.e5. <https://doi.org/10.1016/j.cmet.2017.11.001>.
- Wright, H.J., Hou, J., Xu, B.Z., Cortez, M., Potma, E.O., Tromberg, B.J., and Razorenova, O.V. (2017). CDCP1 drives triple-negative breast cancer metastasis through reduction of lipid-droplet abundance and stimulation of fatty acid oxidation. *Proc. Natl. Acad. Sci. U S A* 114, E6556–E6565. <https://doi.org/10.1073/pnas.1703791114>.
- Wu, X.Y., Deng, F.M., Li, Y.R., Daniels, G., Du, X.X., Ren, Q.H., Wang, J.H., Wang, L.H., Yang, Y., Zhang, V., et al. (2015). ACSL4 promotes prostate cancer growth, invasion and hormonal resistance. *Oncotarget* 6, 44849–44863. <https://doi.org/10.18632/oncotarget.6438>.
- Xu, Y.S., Liang, J.J., Wang, Y.M., Zhao, X.Z.J., Xu, L., Xu, Y.Y., Zou, Q.C., Zou, Q.L.C., Zhang, J.M., Zhang, J.X.M., et al. (2016). STAT3 undergoes acetylation-dependent mitochondrial translocation to regulate pyruvate metabolism. *Sci. Rep.* 6, 39517. <https://doi.org/10.1038/srep39517>.
- Yao, L., Jiang, L.Y., Zhang, F.X., Li, M.H., Yang, B., Zhang, F.T., and Guo, X.Q. (2020). Acetate promotes SNAIL1 expression by ACSL2-mediated histone acetylation under glucose limitation in renal cell carcinoma cell. *Biosci. Rep.* 40, BSR20200382. <https://doi.org/10.1042/bsr20200382>.
- Yuan, H., Li, X., Zhang, X., Kang, R., and Tang, D. (2016). Identification of ACSL4 as a biomarker and contributor of ferroptosis. *Biochem. Biophys. Res. Commun.* 478, 1338–1343. <https://doi.org/10.1016/j.bbrc.2016.08.124>.
- Yuan, Z.L., Guan, Y.J., Chatterjee, D., and Chin, Y.E. (2005). Stat3 dimerization regulated by reversible acetylation of a single lysine residue. *Science* 307, 269–273. <https://doi.org/10.1126/science.1105166>.
- Zinser, E., Sperka-Gottlieb, C.D., Fasch, E.V., Kohlwein, S.D., Paltauf, F., and Daum, G. (1991). Phospholipid synthesis and lipid composition of subcellular membranes in the unicellular eukaryote *Saccharomyces cerevisiae*. *J. Bacteriol.* 173, 2026–2034. <https://doi.org/10.1128/jb.173.6.2026-2034.1991>.

STAR★METHODS

KEY RESOURCES TABLE

REAGENT or RESOURCE	SOURCE	IDENTIFIER
Antibodies		
Mouse monoclonal anti-flag	Sigma Aldrich	F3165; clone M2; RRID: AB_259529
Rabbit monoclonal anti-ACSL4	Thermo Fisher Scientific	PA5-27137; RRID: AB_2544613
Rabbit polyclonal anti-CPT1B	Abcam	ab104662; RRID: AB_10712608
Mouse polyclonal anti-STAT3	Cell Signaling Technology	9139; clone 124H6; RRID: AB_331757
Rabbit polyclonal anti-K685-STAT3	Cell Signaling Technology	2523; RRID: AB_561524
Mouse monoclonal anti-GAPDH	Santa Cruz Biotech	sc-32233; Clone 6C5; RRID: AB_627679
Mouse monoclonal anti-β-actin	Sigma Aldrich	A2228; clone AC-74; RRID: AB_476697
Rabbit polyclonal anti-cleaved caspase 3	Abcam	ab2302; RRID: AB_302962
Normal rabbit IgG	Santa Cruz Biotech	sc-2027; RRID: AB_737197
Normal mouse IgG	Santa Cruz Biotech	sc-2025; RRID: AB_737182
Biological Samples		
Patient breast tumor specimens	City of Hope National Cancer Center	N/A
Chemicals, Peptides, and Recombinant Proteins		
BMS-303141	Sigma-Aldrich	SML0784
3PO	Sigma-Aldrich	SML1343
Doxycycline hyclate	Thermo Fisher Scientific	AC446060050
Perhexiline maleate salt	Sigma-Aldrich	SML0120
RSL3	Selleckchem	S8155
ACSS2 inhibitor	Selleckchem	S8588
MitoTracker Green	Thermo Fisher Scientific	M7514
BODIPY 581/591 C11	Thermo Fisher Scientific	D3861
fatty acid-free BSA and BSA-palmitate	Agilent	102720-100
L-α-Phosphatidylcholine	Sigma-Aldrich	P3782
[³ H]-palmitic acid	PerkinElmer Inc	NET043001MC
[¹⁴ C(U)]- palmitic acid	PerkinElmer Inc	NEC534050UC
acetyl-CoA sodium salt	Sigma-Aldrich	A2056
sodium acetate	Sigma-Aldrich	241245
Paclitaxel	Sigma-Aldrich	T7402
Etomoxir	Sigma-Aldrich	236020
Lipofectamine LTX with PLUS reagent	Thermo Fisher Scientific	15338030
Lipofectamine RNAiMAX transfection reagent	Thermo Fisher Scientific	13778075
PS-acet.-STAT3 peptide	Aftabizadeh et al. (2021)	N/A
PO-acet.-STAT3 peptide	Aftabizadeh et al. (2021)	N/A
Critical Commercial Assays		
Breast tumor tissue array	Biomax US	BR1202
CyQUANT Cell Proliferation Kit	Thermo Fisher Scientific	C7026
PicoProbe acetyl-CoA fluorometric assay kit	BioVision	K317
Deproteinizing Sample Preparation Kit	BioVision	K808-200
Citrate Fluorometric Assay kit	BioVision	K655-10
Pyruvate Fluorometric Assay kit	BioVision	K609
ATP determination kit	Thermo Fisher Scientific	A22066
MitoProbe JC-1 Assay Kit	Thermo Fisher Scientific	M34152
APC- Annexin V assay kit	Biolegend	640932
Mitochondria isolation kit for tissue	Thermo Fisher Scientific	89801
Mitochondria isolation kit for cultured cells	Thermo Fisher Scientific	89874

(Continued on next page)

Continued

REAGENT or RESOURCE	SOURCE	IDENTIFIER
Deposited data		
Differentially expression of fatty acid metabolic genes in MDA-MB-231-R cells expressing WT/KR-STAT3 and in the xenograft tumors treated with PS-acet-STAT3 peptide	This study	GEO: GSE201053
lipidomic analysis upon STAT3 shRNA knockdown	This study	MetaboLights: https://www.ebi.ac.uk/metabolights/studies Study Identifier: MTBLS4709
Expression of lipid metabolic genes in invasive TBNC breast tumors (Figure S2B).	Oncomine (Rhodes et al., 2004)	https://www.oncomine.com/Patient database: CPT1B, Finak Breast; ACADM and ACSL5, Radvanyi Breast; ACSL4, Schuetz Breast
Experimental models: Cell lines		
HCT116	ATCC	CCL-247
MDA-MB-468-Parental	ATCC	HTB-132
MDA-MB-468-Resistant	This study	N/A
MDA-MB-231-Parental	Wang et al., 2018	N/A
MDA-MB-231-Resistant	Wang et al., 2018	N/A
BBM3	Neman et al. (2014)	N/A
Hs578T	ATCC	HTB-126
MDA-MB-436	ATCC	HTB-130
Experimental models: Organisms/strains		
<i>NOD/scid-IL-2Rγcnull</i> NSG mouse	The Jackson Laboratory	Strain #005557
C57BL/6J mouse	The Jackson Laboratory	Strain #000664
Oligonucleotides		
Control siRNA-H siRNA (h)	Santa Cruz Biotech	sc-44236
ACSL4 siRNA (h)	Santa Cruz Biotech	sc-60619
CPT1-M (CPT1-B) siRNA (h)	Santa Cruz Biotech	sc-40382
STAT3 siRNA (h)	Cell Signaling	6580S
All primers used in this study are listed in Table S3	N/A	N/A
Recombinant DNA		
pCMV-6-Myc tag-ACSL4	OriGene	RC205356
pCMV-XL4-CPT1B	OriGene	SC109096
pCMV-6-entry	OriGene	PS100001
pLEGFP-WT-STAT3	Addgene	plasmids # 71449
pLEGFP-K685R-STAT3	Addgene	plasmids # 71450
pLKO-Tet-On	Addgene	plasmid # 21915
STAT3 CRISPR/Cas9 KO	Santa Cruz Biotech	sc-400027
ACSL4 CRISPR/Cas9 KO	Santa Cruz Biotech	sc-401649
CPT1-M (CPT1B) CRISPR/Cas9 KO	Santa Cruz Biotech	sc-401456-KO-2
Software and algorithms		
Zen software	Zeiss	https://www.zeiss.com/microscopy/us/products/microscope-software/zen-lite.html
ImageJ	National Institutes of Health	https://imagej.nih.gov/ij/
Prism	GraphPad software	
ENCODE at UCSC	ENCODE Project	https://genome.ucsc.edu/ENCODE/
Primer-BLAST	National Institutes of Health	https://www.ncbi.nlm.nih.gov/tools/primer-blast/

RESOURCE AVAILABILITY

Lead contact

Further information and requests for resources and reagents should be directed to and will be fulfilled by the lead contact, Dr. Hua Yu (hyu@coh.org).

Materials availability

All reagents generated in this study will be made available on request, but we may require a payment and/or a completed materials transfer agreement if there is potential for commercial application. For non-commercial use, all reagents generated in this study are available from the [lead contact](#) with a completed materials transfer agreement.

Data and code availability

- Differentially expressions of fatty acid metabolic genes in MDA-MB-231-R cells expressing WT/KR-STAT3 and in the xenograft tumors treated with PS-acet-STAT3 peptide have been deposited to GEO repository and are publicly available as of the date of publication. Accession number is listed in the [key resources table](#).

The data of lipidomic analysis upon STAT3 shRNA knockdown has been deposited to MetaboLights and is publicly available as of the date of publication. Study Identifier is listed in the [key resources table](#).

The publicly available mRNA expressions analyzed in [Figure S2B](#) were analyzed from OncoPrint website. The names of these databases are listed in the [key resources table](#).

All data reported in this study will be shared by the [lead contact](#) upon request.

- This paper does not report original code.
- Any additional information required to reanalyze the data reported in this paper is available from the [lead contact](#) upon request.

EXPERIMENTAL MODEL AND SUBJECT DETAILS

Mice

Mouse splenic T cells were isolated from 6–8-week-old male C57BL/6 mice (strain # 000664; The Jackson Laboratory). 6–8-week-old female NSG (*NOD/scid-IL-2R γ c* null; strain # 005557) were used to establish orthotopic TNBC tumor models. All mice were maintained in our Animal Resource Core facility following the guidelines for the Care and Use of Laboratory Animals of the National Institutes of Health. The protocols were approved by the Institutional Animal Care and Use Committee at the Beckman Research Institute at City of Hope (IACUC # 10003 and 08026).

Cell lines

MDA-MB-468 cells were purchased from American Type Culture Collection (ATCC, Manassas, VA, USA) and cultured in DMEM supplemented with 10% FBS, according to vendor's instructions. Parental MDA-MB-231 and BBM3 cells ([Neman et al., 2014](#)) were generated and maintained in DMEM media (Gibco) containing 10% FBS. Chemoresistant MDA-MB-231-R was grown in DMEM containing 10% FBS plus 50 nM paclitaxel (Sigma Aldrich), as previously described ([Wang et al., 2018](#)). Chemoresistant MDA-468-R cells were generated by using a stepwise increase in treatment dose with paclitaxel ([Wang et al., 2018](#)) and finally maintained in the media containing 50 nM of paclitaxel. MDA-MB-436 and Hs578T were gifts from Dr. Hanash's laboratory of MD Anderson Cancer Center. All the cells were maintained in DMEM with 10% FBS. Human HCT116 colon cancer cells were purchased from ATCC and maintained in McCoy's 5A medium with 10% FBS.

Patient breast tumor specimens

Female patient breast tumor specimens were obtained through a City of Hope Institutional Review Board approved protocol with voluntary patient consent. Five female patients with triple negative breast cancer (TNBC) with ages between 45 and 79 (stage 1–4). Each pair of tumor specimens (primary and recurrent) was obtained from the same patient. Clinical and pathologic data were retrieved from medical records under institutionally approved protocols (IRB#09139 at City of Hope). Samples were de-identified to protect patient confidentiality. Paraffin-embedded tissue were obtained from breast tumor resections and prepared as 4 μ m sections on unstained slides for subsequent analysis.

METHOD DETAILS

Cell culture/splenic CD8⁺ T cell isolation

For BSA-palmitate (PA) treatment to restore paclitaxel-induced apoptosis, fatty acid-free BSA and BSA-palmitate (PA) purchased from Agilent (#102720-100; Agilent, Santa Clara, CA, USA) were added to cell culture at 50 μ M. For phospholipid rescue experiment, L- α -Phosphatidylcholine (#P3782; Sigma-Aldrich, St. Louis, MO, USA) was first conjugated with fatty-acid free BSA (4 mg/mL in media) at 125 μ M as described on Sigma-Aldrich website and subsequently added to the cultured cells at 50 μ M.

For doxycycline induced shRNA knockdown, 2 $\mu\text{g}/\text{mL}$ doxycycline was added to induce shRNA knockdown for 5 d in shSTAT3 and shACSL4 stable transformation breast cancer cells. Doxycycline was replenished by media change on day 3 to maintain shRNA production until day 5.

For siRNA transfection, the cells were seeded to be 60 to 80 confluent one day before siRNA transfection. Then, siRNA transfection was performed using Lipofectamine RNAiMAX transfection reagent (#13778075, Thermo Fisher Scientific, Boston, MA, USA), following manufacturers' instructions. siRNA transfection was repeated on day 3 for another 2 days to ensure knockdown efficiency.

For CRISPR/Cas9 KO plasmid transfections, calcium phosphate (CalPhos Mammalian Transfection Kit; # 631312; Takara Bio inc, Kusatsu, Shiga, Japan) was used for large scale DNA transfection. The DNA transfection was optimized to ensure the high efficiency. Because long term gene perturbation of STAT3, ACSL4 or CPT1B causes cell death, the KO cells (GFP + cells) were harvested to establish orthotopic xenograft tumors after 3 d of DNA transfection.

For ectopic ACSL4 and CPT1B expression, control or cDNA containing plasmids were transfected to the cells using Lipofectamine LTX with PLUS reagent (#15338030; Thermo Fisher Scientific). After 2 d of DNA transfection, the cells were harvested for the experiments.

For determining the level of acetyl-STAT3 by acetate or acetyl-CoA, 20 mM of acetate (sodium acetate, #241245, Sigma) or 5 μM of acetyl-CoA (acetyl-CoA sodium salt, #A2056, Sigma) was added to cultured cells as indicated for 6 h or 16 h, respectively, and the levels of acetyl-STAT3, total STAT3, CPT1B and ACSL4 were determined by western blotting. For ACSS2 inhibitor treatment, 10 μM of ACSS2 inhibitor (S8588, Selleckchem, Houston, TX, USA) was added in flag-WT or KR-STAT3 expressing MDA-MB-231-R cells for 2 h preincubation. After acetate incubation at 37°C for 6 h, the level of acetyl-STAT3 was then measured by immunoprecipitation and western blotting.

For investigating the protein levels of acetyl-STAT3 in MDA-MB-231-R cells treated with vehicle, ACLY inhibitor (ACLYi, BMS-303141, #SML0784, Sigma-Aldrich) or PFKFB3 inhibitor (PFKFB3i; 3PO, #SML1343, Sigma-Aldrich) for 2 d.

For evaluating the effects of PS-acet.-STAT3 peptide on MDA-MB-231-R, MDA-MB-468-R, MDA-MB-231-P or ACSL4 overexpressing MDA-MB-231-P cells, 10 μg of PS-acet.-STAT3 peptide (0.33 μM) was added to cultured cells for 5 d before assessing expression of CPT1B and ACSL4, FAO, mitochondrial $\Delta\psi$ or apoptosis assay.

Spleens from C57BL/6 mice were excised, gently minced and incubated in 400 U/mL of Collagenase D/DNase I solution (Roche, Basel, Switzerland) for 15 min at 37°C. Cell suspensions were filtered through a mesh filter (70 μm). Red blood cells were lysed, using an RBC lysis buffer (#11814389001; Sigma) and the cells were resuspended in 10 mL of HBSS containing 2% FBS. CD8⁺ T cells were isolated using MojoSort mouse CD8⁺ T cell isolation kit (480007; Biolegend, San Diego, CA, USA), according to manufacturer's instruction.

Plasmids and siRNAs

The DNA plasmids used in this study are: pCMV-6-Myc tag-ACSL4 (RC205356), pCMV-6-entry (PS100001) and pCMV-XL4-CPT1B (SC109096) were purchased from OriGene (Rockville, MD) and used for ectopic ACSL4 and CPT1B expression. pCMV-6-entry was used as controls for DNA transfection. pLEGFP-WT-STAT3 and pLEGFP-K685R-STAT3 were gifts from George Stark (plasmids # 71449 and 71450; GFP tag was replaced with flag tag, Addgene, Watertown, MA, USA). pLKO-Tet-On vector was a gift from Dmitri Wiederschain (Addgene plasmid # 21915) and used to generate doxycycline-induced shRNAs targeting STAT3 and ACSL4 (shSTAT3 and shACSL4). The sequences of the oligos used for generating shRNAs are listed in [Table S3'](#).

STAT3 CRISPR/Cas9 KO (#sc-400027), ACSL4 CRISPR/Cas9 KO (#sc-401649) and CPT1-M (CPT1B) CRISPR/Cas9 KO (#sc-401456-KO-2) plasmids were purchased from Santa Cruz Biotechnology (Dallas, TX, USA).

ACSL4 siRNA (#sc-60619), CPT1-M (CPT1B) siRNA (#sc-40382) and control siRNA-H (#sc-44236) were purchased from Santa Cruz Biotechnology. STAT3 siRNA (#6580S) was purchased from Cell Signaling (Danvers, MA, USA).

Mitochondrial DNA quantification

The cells were washed with 1 \times PBS, centrifuged at 1500 rpm for 5 min at 4°C. The total DNA was extracted by using DNeasy Blood & Tissue Kit (# 69,504, Qiagen, Hilden, Germany), following manufacturer's instructions. Quantification of mitochondrial DNA was performed by qPCR with SYBR green-based detection (Thermo Fisher Scientific). Relative mDNA:nDNA ratio was calculated using the ΔCt method upon targeting of nuclear-encoded genes (human B2M) and mitochondrial-encoded genes (human tRNALeu) ([Jasoliya et al., 2017](#)). The sequences of the primers are listed in [Table S3](#).

In vivo experiments

Mouse care and experimental procedures were performed under pathogen-free conditions in accordance with established institutional guidance and an approved IACUC protocol (10003) from Research Animal Care Committees of the City of Hope. For STAT3 or ACSL4 knockdown experiment, 1 \times 10⁶ MDA-MB-231-R cells transformed with doxycycline-induced shRNA targeting STAT3 or ACSL4 were mixed with Matrigel and injected into mammary fat pad in female NSG (*NOD/scid-IL-2R γ c* null) mice maintained in the Animal Resource Core at the Beckman Research Institute at City of Hope. Three days post tumor implantation, the tumor bearing mice were randomly divided into two groups. One group ($n = 5$) of mice was switched to doxycycline containing diet (Dox+) (#TD.01306; Envigo, Indianapolis, IN, USA) while the other group remained on the normal diet (Dox-). Tumor growth was measured by a digital caliper twice a week.

For STAT3, ACSL4 or CPT1B KO experiments, GFP positive 1×10^6 MDA-MB-231-R or MDA-MB-231-R KO cells with CRISPR/Cas9 targeting STAT3, ACSL4 or CPT1B were mixed with Matrigel (356231, Corning, Tewksbury, MA, USA) and injected into mammary fat pad in female NSG mice. Tumor growth was measured by a digital caliper twice a week.

For PS-acet.-STAT3 peptide treatment, 5×10^6 MDA-MB-231-R cells were injected into mammary fat pads of female NSG mice. When tumors reached an average size of 80–100 mm³, mice ($n = 4$) were intravenously treated with 1 mg/kg of PS-acet.-STAT3 peptide (AnaSpec, Fremont, CA, USA) or vehicle (HBSS; Thermo Fisher Scientific) every other day. Tumor growth was measured by a digital caliper every other day. To study the effects of the modified peptides at protein and gene levels, mice were euthanized when the tumor size reached to 500 mm³ in control groups.

Immunoblotting and immunoprecipitation

Whole cell lysates or tissue homogenates were prepared by using RIPA lysis buffer (50 mM Tris, pH 7.4, 150 mM NaCl, 1 mM EDTA, 0.5% NP-40, 1 mM NaF, 15% glycerol, and 20 mM β -glycerophosphate). A protease inhibitor cocktail (Mini Protease Inhibitor Cocktail; Roche) and a tyrosine phosphatase inhibitor, sodium orthovanadate (Na_3VO_4 , 1 mM) were added freshly to the lysis buffer. Protein amounts were determined by BCA using a Thermo fisher scientific kit (# 23225). Normalized protein amounts were subjected to an SDS-PAGE and transferred onto a nitrocellulose membrane for western blotting. Proteins were visualized with a Chemi-luminescent Detection Kit (SuperSignal West Femto Maximum Sensitivity Substrate; 34094; Thermo Fisher Scientific). In addition, primary antibodies against STAT3 (#9139, 124H6) and acetyl-K685-STAT3 (#2523) were purchased from Cell Signaling Technology. Anti- β -actin from Sigma-Aldrich (AC-74; #A2228). Anti-GAPDH (6C5; #sc-32233), anti-cleaved caspase 3 (Abcam, #ab2302) and anti-CPT1B (#ab134988) were purchased from Santa Cruz Biotechnology and Abcam (Cambridge, United Kingdom), respectively. Anti-ACSL4 (PA5-27137) was obtained from Thermo Fisher Scientific. Amersham ECL HRP-conjugated antibodies were used as the secondary antibodies (#NA934 and #NA931, Amersham Bioscience Corp. Amersham, United Kingdom). For immunoprecipitation, 2 μ g of anti-STAT3 or anti-flag antibody (M2, #F3165, Sigma-Aldrich) was used to incubate with 100 μ g precleared cell lysates at 4°C overnight. Recombinant protein G agarose beads (#15920010; Thermo Fisher Scientific) were then added to pull down antibody-antigen complex. After three washes with 1 \times RIPA buffer, samples were subjected to SDS-PAGE followed by western blotting or scintillation counting.

For protein quantification from western blots, the levels of acetyl-STAT3 were quantified normalized with total STAT3 and the level of ACSL4, CPT1B and cleaved caspase 3 were quantified and normalized with GAPDH or β -actin by band intensity of western blotting using ImageJ software (National Institutes of Health, Public Domain, BSD-2) as indicated.

The protein level of STAT3 and ACSL4 in the individual xenograft tumors was assessed by western blotting. The protein levels were quantified by band intensity of western blotting and normalized with β -actin. The relative protein levels in the tumors with knockdown were further normalized with the mean of the protein levels in the tumors without knockdown and the data is shown in bar graphs.

Fluorescent microscopy imaging

IF staining for mitochondrial $\Delta\psi$ was carried out by seeding 1×10^4 of MDA-MB-231-R cells per well of an 8-well chamber slide (Nunc Lab-Tek II, #154534PK, Thermo Fisher Scientific) and incubated with 10 nM of perhexiline (#SML0120, Sigma-Aldrich) for 16 h. In addition, 1×10^4 of MDA-MB-231-R cells transformed with doxycycline-inducible shRNA or transfected with siRNA targeting STAT3 or ACSL4 were also seeded in a well of the chamber slide. After 5 d of doxycycline-induced shRNA knockdown or 16 h post perhexiline treatment, mitochondrial $\Delta\psi$ was visualized by JC1 staining (MitoProbe JC-1 Assay Kit, #M34152, Thermo Fisher Scientific).

For fluorescent IHC staining, the xenograft tumor tissues were collected, and part of tissues were embedded in OCT block. The tissue sections from the OCT-frozen tumor tissues were fixed in 2% formaldehyde and permeabilized with methanol and blocked in PBS containing 5% FBS (Sigma-Aldrich). Samples were stained at 4°C overnight with primary antibodies to acetyl-STAT3 (Lys685, #2523; Cell Signaling), ACSL4 (F4; #sc-365230; Santa Cruz Biotechnology), Ki-67 (Cell signaling technology, D3B5, #12202), FITC (also binds to FAM) (Abcam, #ab19224) and cleaved caspase 3 (Abcam, #ab2302). The fluorophore secondary antibodies were from Invitrogen. The nuclei were stained with Hoechst 33342. After staining with antibodies, slides were mounted and analyzed by confocal microscopy. The confocal imaging was carried out using a 40 \times or 20 \times immersion objective on LSM 700 confocal microscope (Zeiss, Oberkochen, Germany). Images were analyzed and quantified using Zen software (Zeiss).

For tissue array samples (BR1202, only TNBC tumor tissues were examined; Biomax US, Rockville, MD, USA) or patient tumor sections (Solid Tumor Core, City of Hope), paraffin-embedded tumor or normal breast tissues were deparaffinized, rehydrated through an alcohol series, and then boiled in Antigen Unmasking Solution (Tris-based; #H-3301-250; Vector Laboratories, Burlingame, CA, USA). After incubation with a blocking solution, the sections were stained overnight at 4°C with a 1:100 dilution of the indicated primary antibody, and then 1:200 dilution of a secondary antibody. The images were obtained by confocal microscopy. The images were quantified by Zen software (Zeiss) and presented as the mean of fluorescent intensity (M.F.I). Cytokeratin was co-stained as a tumor cell marker. M.F.I of acetyl-STAT3 or cytokeratin was normalized with Hoechst 33342 in the plot.

Cell proliferation assay

Cell proliferation was measured by using CyQUANT Cell Proliferation Kit (#C7026, Thermo Fisher Scientific). In brief, 1×10^4 of MDA-MB-231-R cells were seeded per well in a 96-well plate for phospholipid rescue experiment. After 1 day, cells were treated with 75 nM of

paclitaxel along with vehicle or 50 μ M of PC phospholipids for 48 h or left untreated as a control. The cell proliferation was measured according to manufacturer's instruction. A reference standard curve (based on different cell numbers) was generated in the same assay plate for converting sample fluorescence values into cell numbers. For ACLY inhibitor testing, 10 μ M of BMS-303141 (SML0784, Sigma-Aldrich) was added to cell culture and the cell proliferation was examined as described above after 48 h treatment.

To determine whether ACSL4 overexpression in parental MDA-MB-231 cells can restore cell survival upon paclitaxel treatment. The control or ACSL4 overexpressing cells were treated with 75 nM of paclitaxel for 48 h before CyQUANT assay.

Acetyl-CoA assay

The level of acetyl-CoA was examined by using a PicoProbe acetyl-CoA fluorometric assay kit (#K317; BioVision, Milpitas, CA, USA) in parental MDA-MB-231 cells with ectopic CPT1B expression, FAO blocking by 100 μ M of etomoxir and 10 nM of perhexiline or in the MDA-MB-231-R cells with STAT3 and CPT1B siRNA knockdown for 5 d. The assay was performed following manufacturers' instructions. In brief, 1×10^6 cells were lysed with 100 μ L of acetyl-CoA Assay Buffer. Cell debris were removed by centrifugation at 15,000 g for 10 min. Further, protein was removed by using a Deproteinizing Sample Preparation Kit (#K808-200, BioVision). Next, 10 μ L of sample was loaded into triplicated wells of a 96-well plate and 40 μ L of assay buffer was added to bring volume to 50 μ L. Standard samples were loaded into duplicated wells of a 96-well plate. Free CoASH, malonyl CoA, and succ-CoA in samples generate background. In order to correct for this background, 10 μ L of CoA Quencher was added to each standard and testing sample to quench free CoA. Incubate for 5 min at room temp. Then 2 μ L of Quench Remover was added and 5 min. Subsequently, 50 μ L of the reaction mix (conversion enzyme, enzyme mix, substrate mix, PicoProbe and assay buffer) was added to each well containing the citrate standard and test samples and the reaction mixture was incubate for 10 min at room temperature. The fluorescence was measured at Ex/Em = 535/587nm in a microplate reader (Cytation 5, BioTek, Winooski, VT).

Citrate fluorometric assay

The experiments were performed by using Citrate Fluorometric Assay kit (#K655-10, BioVision) and following manufacturer's instructions. In brief, 2×10^6 parental and chemoresistant MDA-MB-231-R or MDA-MB-468-R cells were lysed with 100 μ L of Citrate Assay Buffer. Cell debris were removed by centrifugation at 15,000 g for 10 min. Further, protein was removed by using a Deproteinizing Sample Preparation Kit (#K808-200, BioVision). Next, 50 μ L of sample was loaded into triplicated wells of a 96-well plate. Standard samples were loaded into duplicated wells of a 96-well plate. Subsequently, 50 μ L of the reaction mix (citrate enzyme mix, developer, citrate probe and citrate assay buffer) was added to each well containing the citrate standard and test samples and the reaction mixture was incubate for 30 min at room temperature. The fluorescence was measured at Ex/Em = 535/587nm in a microplate reader (Cytation 5, BioTek). For determining the citrate level in STAT3 or CPT1B knockdown MDA-MB-231-R cells, the same approaches were used as described above after siRNA knockdown for 5 d.

Pyruvate fluorometric assay

The experiments were performed by using Pyruvate Fluorometric Assay kit (#K609, BioVision) and following manufacturer's instructions. In brief, 2×10^6 parental and chemoresistant MDA-MB-231-R or MDA-MB-468-R cells were lysed in 4 volumes of the pyruvate assay buffer. Cell debris was removed by centrifugation (10,000 \times g; 10 min; 4°C). Further, protein was removed by using a Deproteinizing Sample Preparation Kit (#K808-200, BioVision). Next, 50 μ L of sample was loaded into triplicated wells of a 96-well plate. Standard samples were loaded into duplicated wells of a 96-well plate. Subsequently, 50 μ L of the reaction mix (enzyme mix, pyruvate probe and pyruvate assay buffer) was added to each well containing the pyruvate standard and test samples and the reaction mixture was incubate for 30 min at room temperature. The fluorescence was measured at Ex/Em = 535/590nm in a microplate reader (Cytation 5, BioTek).

ATP-based bioluminescence assay

Mitochondrial was isolated from MDA-MB-231-R cells (1×10^6) treated with 10 μ g of PO-acet.-STAT3 or PS-acet.-STAT3 peptide for 5 d. The peptide treatment was replenished every day. The level of mitochondrial ATP was measured by an ATP determination kit (#A22066; Thermo Fisher Scientific) following manufactures' instructions.

Quantitative real-time PCR (qPCR)

Total RNA was extracted from cultured or tumor tissues using RNasy kit (Qiagen), according to manufacturer's instruction. After cDNA synthesis using iScript cDNA Synthesis kit (Bio-Rad, Hercules, CA, USA), samples were analyzed using pairs of primers specific for *ACSL4*, *CPT1B*, *BCL2L1*, *MYC*, *CDKN2A* as indicated. Sequence-specific amplification was detected by fluorescent signal of SYBR Green (iQ SYBR Green Supermix, 1708880, Bio-Rad) by using CFX96 Real-time PCR Detector (Bio-Rad). Real-time PCR was performed in triplicate using the CFX96 Real-Time Detector (Bio-Rad). The human *GAPDH* or *ACTB* housekeeping gene was used as an internal control to normalize target gene mRNA levels. Primers are ordered from Integrated DNA Technologies and the sequences are listed in [Table S3](#).

Microarray analysis

WT or K685R mutant-STAT3 was ectopically expressed in MDA-MB-231-R cells through DNA transfection. After 48 h of DNA transfection, cells were harvested, and RNA was isolated by using RNeasy Plus Kits (#74134; Qiagen). Reverse transcription was

performed using 1000 ng total RNA using iScript cDNA synthesis kit (1708891; Bio-Rad). PCR assays were performed by using Human Fatty Acid and Lipid Metabolism Primer Library (HFLM-1; RealTimePrimers, LLC, Melrose Park, PA, USA). Quantitative real-time PCR were performed (CFX96, Bio-Rad) with 45 cycles at 94°C for 15 s and 60°C for 60 s. For the differential expression of lipid metabolic genes in MDA-MB-231-R (paclitaxel-resistant) xenograft tumors that had been treated with HBSS or PS-acet-STAT3 peptide, RNA was isolated from pooled tumor tissues (n = 4) by using RNeasy Plus Kits. Reverse transcription and PCR assays using Human Fatty Acid and Lipid Metabolism Primer Library were performed as described above.

Chromatin immunoprecipitation (ChIP) assay

ChIP assay was performed as described previously (Carey et al., 2009; Wang et al., 2018). We identified STAT3 as a transcription factor that directly binds to the CPT1B promoter (chr22:51,017,100) (Wang et al., 2018). For *ACSL4*, *ACADM* and *ACSL5* gene regulation, STAT3 has been shown to bind to their promoter region in breast MCF-10A cells (chrX:108978487-108978746, chr1:76187965-76188280 and chr10:114120643-114121009, respectively) by transcription factor ChIP-seq from ENCODE project (UCSC, <https://genome.ucsc.edu/ENCODE/>). The primers around the consensus STAT3 binding sites (Khan et al., 2018) were designed by using NIH Primer-BLAST (<https://www.ncbi.nlm.nih.gov/tools/primer-blast/>). Quantitative real-time PCR (qPCR) reactions were performed with ChIP-bound and input DNA. qPCR was performed as described above. The resulting signals were normalized with input DNA. The sequences of oligo primers used in the study are listed in Table S3.

¹⁴C-palmitic acid labeling

MDA-MB-231-R cells were preincubated with vehicle, 10 nM of perhexiline, 10 μM of ACLY or 10 μM of glycolysis inhibitor 3PO for 2 h in low glucose DMEM medium and 2% fatty acid-free BSA for 2h before 0.5 mM palmate, 1 mM carnitine, and 0.5 μCi/mL [¹⁴C(U)]-palmitic acid (#NEC534050UC, PerkinElmer, Waltham, MA, USA) were added to the cell culture for another 8 h incubation at 37°C. Subsequently, the cells were harvested to determine ¹⁴C labeling of STAT3 after washing in PBS. The cells were lysed in 1 × RIPA buffer and ¹⁴C-STAT3 protein was pulled down by anti-STAT3 antibody (124H6, #9139, Cell Signaling) and protein G beads (#15920010; Thermo Fisher Scientific) as described in immunoprecipitation section. After four washes in 1 × RIPA buffer, the level of ¹⁴C-labeled STAT3 was quantified by scintillation counting.

For WT or KR-STAT3 expressing cells, the ¹⁴C-palmitic acid tracing was performed as described above except the antibody used for immunoprecipitation was anti-flag antibody.

Thin-layer chromatography (TLC)

Lipids were loaded, together with standards (Avanti), onto unmodified Silica Gel TLC plates (Sigma-Aldrich) preheated at 80°C for 15 m. The lipids were separated for 45 to 60 m, using a mobile phase of chloroform-ethanol-water-triethylamine (30:35:7:35, v/v) for phospholipids. Lipid spots were visualized under ultraviolet light after staining the plate with primuline solution (0.005%). The lipid standards (PC, PS, PI, PE and CL) for TLC were obtained from Avanti. A ChemiDoc imager (Bio-Rad) was then used to detect and quantify the lipid spot.

Mitochondria preparation

For cultured cells, mitochondria were isolated by differential centrifugation using a commercial kit available from Thermo Scientific (mitochondria isolation kit for cultured cells; #89874). Briefly, the homogenate was prepared from 2 × 10⁷ cells using Reagent B and centrifuged at 700 g for 10 m at 4°C. Mitochondria-rich supernatant was then centrifuged again at 12,000 g for 15 m to enriched mitochondria. The pellet was then washed with reagent C and the final pellet was gently resuspended in mitochondria isolation reagent provided by the manufacturer.

For tumor tissues, mitochondria from xenograft tumors were isolated by reagent-based method using a commercially available kit (mitochondria isolation kit for tissue; #89801; Thermo Fisher Scientific). In brief, 100 to 200 mg of tumor tissue was washed with PBS twice prior to disrupt tissue in 800 μL of PBS. The tissue homogenate was then centrifuged at 1,000 g for 3 m at 4°C and discard the supernatant. The pellet was suspended in 800 μL of BSA/reagent A solution. After vortexing for 2 m, 10 μL of Mitochondria Isolation reagent B was added to the samples and the samples were kept on ice for 5m. 800 μL of Mitochondria Isolation reagent C was then added to the samples and differential centrifugation was used to extract the mitochondria following manufacturer's instructions.

JC-1 staining of mitochondrial Δψ

JC-1 dye was dissolved at 1 mM in DMSO as instructed by the manufacturer (ab113850; Abcam) and a 1/500 volume was diluted in dilution buffer and added to 1 × 10⁶ cells in 1 mL culture medium for flow cytometry or to 2 × 10⁴ cells in 100 μL medium for fluorescent microscopy assay. JC1 dye was incubated with cells at 37°C for 30 m in dark and mitochondrial Δψ was assessed by flow cytometry or fluorescent microscopy after briefly washed cells with warm medium or PBS.

For fluorescent microscopy assay, MDA-MB-231-R cells were treated with either vehicle or 10 nM of perhexiline 16 h or induced shRNA silencing of STAT3 or ACSL4 for 5 d. before mitochondrial Δψ was assessed by JC1 staining. The graphs shown are relative mean of fluorescence intensity (MFI) of JC1 red/JC1 green assessed by confocal microscopy and quantified by Zen software (Zeiss).

To induce mitochondrial membrane depolarization, cells were treated with 100 μM of carbonyl cyanide 4- (trifluoromethoxy) phenylhydrazone (FCCP) for 5 m prior to adding JC-1 dye. After wash in warm 1 × PBS to remove remaining JC1 dye, fluorescence data

were collected on an Attune NxT flow cytometer (Thermo Fisher Scientific) and analyzed using FlowJo software. Mitochondrial $\Delta\psi$ was measured by relative ratio of aggregate (red) and monomeric (green) forms of mitochondria (red/green ratio). For JC1 staining coupled with APC-Annexin-V staining, 5 μ L of APC-Annexin V was added to the samples already stained with JC1 as described above and further incubated for 15 min at 37°C. After that, Annexin-V binding buffer was added to dilute Annexin-V and the samples were examined by using Attune NxT flow cytometer (Thermo Fisher Scientific) and analyzed using FlowJo software.

For palmitate or phospholipid PC rescue experiments, 3×10^5 of parental or MDA-MB-231-R cells were seeded per well of 6-well culture plate. 50 μ M of BSA or BSA-palmitate (PA) was added to parental MDA-MB-231 cell culture for 3 d before paclitaxel (50 nM) was added to induce apoptosis for 24 h. 50 μ M of BSA (vehicle) or BSA-phospholipid PC (PC) was added to MDA-MB-231-R cell culture for 3 d before paclitaxel (75 nM) was added to induce apoptosis for 48 h. Control cells were left untreated (Ctrl). The changes of mitochondrial $\Delta\psi$ were examined by JC1 staining and flow cytometry as described above.

MitoTracker green labeling

MitoTracker Green was obtained from Thermo Fisher Scientific at 1 mM in DMSO (M7514). The stock was added to the MDA-MB-231-R cells with or without STAT3 or ACSL4 or ACSL4 overexpressing cells for 15 min at 37°C at 25 nM final concentration. After staining, the cells were washed with warm media to remove the excess dye and visualized by confocal microscopy. The mean of fluorescent intensity was quantified by Zen software (Zeiss).

Fatty acid oxidation assay

The experiment procedures were the same as described in our previous study (Wang et al., 2018). In brief, 1×10^6 cells of parental or chemoresistant MDA-MB-231 or MDA-MB-468 cells were washed three times with HBSS. Then, 200 μ L of [³H]-palmitic acid (1 mCi/mL, NET043001MC, PerkinElmer Inc) bound to fatty-acid free albumin (100 μ M; the ratio of palmitate: albumin is 2:1) and 1 mM L-carnitine were added to each well. Incubation was carried out for 2 h at 37°C. After incubation, the media was collected and added to a tube containing 200 μ L of cold 10% trichloroacetic acid. The tubes were centrifuged 10 min at 3,000g at 4°C and aliquots of supernatants (350 μ L) were removed, neutralized with 55 μ L of 6N NaOH, and applied to an ion exchange column loaded with Dowex 1 \times 2 chloride form resin (C4650, Sigma-Aldrich). The radioactive product was eluted with water. Flow-through was collected and radiation was quantified using liquid scintillation counting. Radiation count was normalized to amount of protein, as quantified by BCA assay (#23225, Thermo Fisher Scientific).

For peptide treatment, 10 μ g of PO- or PS-acet.-STAT3 peptide was added to 1×10^6 cells and replenished every day for 5 d before fatty acid oxidation was analyzed as described above.

Ferroptosis assay

ACSL4 or STAT3 gene was knockdown by doxycycline-induced shRNA in MDA-MB-231-R cells and ferroptosis was performed using BODIPY 581/591 C11 (lipid peroxidation sensor; D3861, Thermo Fisher Scientific) as described in a previous study (Martinez et al., 2020). In brief, 2 μ L of 1.5 mM BODIPY 581/591 C11 stock solution to 2 mL of cell culture media and further incubated with cells for 20 min in cell culture incubator. 1 μ M of RSL3 (S8155; Selleckchem, Houston, TX, USA) was used to induce ferroptosis as a positive control. After staining, the cells were washed, and the data were collected by flow cytometry as described above.

Annexin V/PI apoptosis assay

MDA-MB-231-R cells were treated with either vehicle or 10 nM of perhexiline 16 h or induced shRNA silencing of STAT3 or ACSL4 for 5 d. Then, the cells were stained with 5 μ L of APC-conjugated Annexin V and PI in 100 μ L binding buffer provided by Biologend for 15 min at 37°C (#640932) and the samples were briefly washed in warm PBS before analyzing by flow cytometry.

Lipid analysis-Mass spectrometry

Metabolites were extracted from flash frozen cell pellets through the addition of 1 mL of pre-chilled 3:1 isopropanol:ultrapure water. Samples were briefly vortexed followed by centrifugation at 4°C for 10 min at 2,000 \times g. Thereafter, metabolite extracts were transferred to 1.5 mL Eppendorf tubes and stored at -20°C until metabolomic analysis.

For analysis of complex lipids, 10 μ L (3:1 isopropanol:ultrapure water) of the cell lysates supernatant was diluted with 90 μ L of 1:3:2 100mM ammonium formate, pH3: acetonitrile: 2-propanol (Fisher Scientific) and transferred to a 384-well microplate (Eppendorf) for analysis by LC-MS. Untargeted lipidomics analyses were conducted on a Waters Acquity UPLC system coupled to a Xevo G2-XS quadrupole time-of-flight (qTOF) mass spectrometer. Chromatographic separation was performed using a C18 (Acquity™ UPLC HSS T3, 100 Å, 1.8 μ m, 2.1 \times 100mm, Water Corporation, Milford, U.S.A) column at 55°C. The mobile phases were: (A) water, (B) Acetonitrile, (C) 2-propanol and (D) 500mM ammonium formate, pH 3. A starting elution gradient of 20% A, 30% B, 49% C and 1% D was increased linearly to 10% B, 89% C and 1% D for 5.5 min, followed by isocratic elution at 10% B, 89% C and 1% D for 1.5 min and column equilibration with initial conditions for 1min.

Mass spectrometry data was acquired using 'sensitivity' mode in positive and negative electrospray ionization mode within 100–2000 Da for complex lipids. For the electrospray acquisition, the capillary voltage was set at 1.5 kV (positive), 3.0kV (negative), sample cone voltage 30V, source temperature at 120°C, cone gas flow 50 L/h and desolvation gas flow rate of 800 L/h with scan time of 0.5 s in continuum mode. Leucine Enkephalin; 556.2771 Da (positive) and 554.2615 Da (negative) was used for lockspray correction and

scans were performed at 0.5 min. The injection volume for each sample was 3 μ L. The acquisition was carried out with instrument auto gain control to optimize instrument sensitivity over the sample acquisition time.

LC-MS and LC-MSe data were processed using Progenesis Q1 (Nonlinear, Waters) and values were reported as area units. Annotations were determined by matching accurate mass and retention times using customized libraries created from authentic standards and/or by matching experimental tandem mass spectrometry data against the NIST MSMS or HMDB v3 theoretical fragmentations; for complex lipids, retention time patterns that are characteristic of discrete lipid species were also considered (Aicheler et al., 2015).

To correct for injection order drift, each feature was normalized using data from repeat injections of quality control samples collected every 10 injections throughout the run sequence. Measurement data were smoothed by Locally Weighted Scatterplot Smoothing (LOWESS) signal correction (QC-RLSC) as previously described (Wang et al., 2018). Metabolite feature values between quality control samples were interpolated by a cubic spline. Metabolite values were rescaled by using the overall median of the historical quality control peak areas across all samples. Only detected features exhibiting a relative standard deviation (RSD) less than 30 in either the historical or pooled quality controls samples were considered for further statistical analysis. To reduce data matrix complexity, annotated features with multiple adducts or acquisition mode repeats were collapsed to one representative unique feature. Features were selected based on replicate precision (RSD<30), highest intensity and best isotope similarity matching to theoretical isotope distributions. Values are reported as normalized area units.

Oligopeptide structure and synthesis

PO- or PS-acet.-STAT3 peptides were produced by AnaSpec (Fremont, CA, USA) and Eurogenetec (Seraing, Belgium). The structures and sequences of PS- and PO-acet.-STAT3 peptides were described in our previous publication (Aftabizadeh et al., 2021). In brief, phosphorothioated (PS)-polymer modified STAT3 peptides span 22 amino acids of STAT3 protein (amino acids 675–697) including Lysine 685 (K685). Acetyl-STAT3 peptide (PS-acet.-STAT3 pept.) is generated by adding an acetyl group to lysine 685. PO-acet.-STAT3 is acetyl-STAT3 peptide conjugated to non-phosphorothioated polymer backbone.

Peptide penetration

Peptide penetration assays were performed on patient primary BBM3 tumor spheres. BBM3 tumorsphere were generated and maintained as previously described (Wang et al., 2018). In brief, BBM3 tumorspheres were cultured in DMEM/F12 supplemented with 2% B27 (Life Technologies), 20ng/mL hEGF, 20ng/mL hFGF2 (Peprotech), and heparin in a suspension cell culture flask. Tumorspheres were then treated with 0.33 μ M of FAM-labeled PO- or TAMRA-labeled PS-conjugated peptides for 2 h at 37°C. The penetrating efficacy was examined by fluorescent microscopy.

QUANTIFICATION AND STATISTICAL ANALYSIS

All *in vitro* experiments were done at least three independent times as indicated in figure legends. Statistical analyses were performed using Prism (version 9, GraphPad software, San Diego, CA, USA) software. n = the number of biological replicates, tumors or mice as indicated in figure legends and Table S1. Two tailed/unpaired student's t test was used to calculate statistical differences between any two groups. One-way ANOVA was used to calculate statistical differences between any three or more groups. two-way ANOVA (Tukey's multiple-comparisons test) was used for analyzing the kinetic of tumor growth. p values were shown in figures and/or legends with asterisks. ****, $p < 0.001$; ***, $p < 0.005$; **, $p < 0.01$; *, $p < 0.05$. p values of less than 0.05 were considered not statistically significant.

Cell Reports, Volume 39

Supplemental information

**Fatty acid oxidation protects cancer cells
from apoptosis by increasing
mitochondrial membrane lipids**

Yi-Jia Li, Johannes Francois Fahrman, Maryam Aftabizadeh, Qianqian Zhao, Satyendra C. Tripathi, Chunyan Zhang, Yuan Yuan, David Ann, Samir Hanash, and Hua Yu

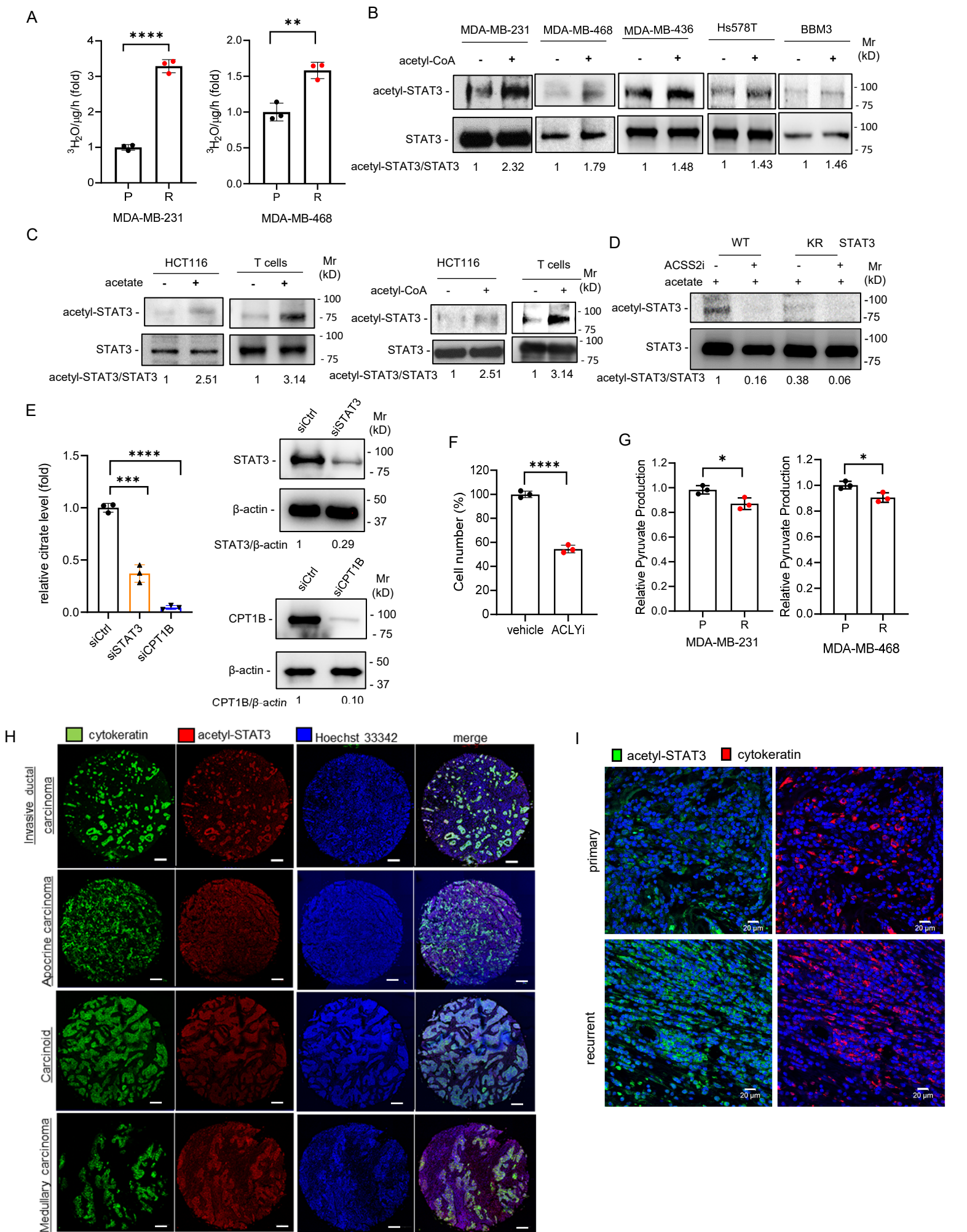


Figure S1. Acetyl-CoA metabolized from FAO is required for STAT3 acetylation, related to Figure 1.

(A) FAO assay comparing of FAO levels in parental (P) and chemoresistant (R) MDA-MB-231 and MDA-MB-468 cells. Shown are mean \pm SD (n=3 biological replicates). Two tailed, unpaired student's t test. **, P<0.01; ****, P<0.001.

(B) Acetyl-CoA was added to indicated cultured cells for 16 h. An increase in acetyl-STAT3 was determined by western blotting. For MDA-MB-231, MDA-MB-468 and mouse splenic T cells, immunoprecipitation (anti-STAT3) and western blotting were used to assess and confirm the increased acetyl-STAT3.

(C) Acetate or acetyl-CoA was added to cultured HCT116 and mouse splenic T cells for 6 or 16h, respectively. An increase in acetyl-STAT3 was detected by western blotting.

(D) Prior to acetate incubation, 10 μ M of ACSS2 inhibitor was added in flag-WT or KR-STAT3 expressing MDA-MB-231-R cells for 2 h preincubation. After acetate incubation at 37°C for 6 h, the level of acetyl-STAT3 was then measured by immunoprecipitation using anti-flag antibody and western blotting.

(E) Left panels, relative citrate levels were measured by citrate colorimetric assay in MDA-MB-231-R cells after 5 d of siRNA-mediated STAT3 (siSTAT3) and CPT1B (siCPT1B) knockdown. Control siRNA (siCtrl) was used as a control. Shown are mean \pm SD (n=3 biological replicates). Two tailed, unpaired student's t test. ****, P<0.001; ***, P<0.005. Right panels, the protein levels of STAT3 and CPT1B after 5 d of gene knockdown were examined by western blotting.

(F) The effects of ACLYi (BMS-303141) on cell proliferation in MDA-MB-231-R cells after 2 d treatment was determined by CyQUANT assay. Shown are mean \pm SD (n=3 biological replicates). Two tailed, unpaired student's t test. ****, P<0.001.

(G) Relative pyruvate levels were measured in parental (P) and chemoresistant (R) MDA-MB-231 and MDA-MB-468 cells by pyruvate colorimetric assay kit. Shown are mean \pm SD (n=3 biological replicates). Two tailed, unpaired student's t test. *, P<0.05.

(H) The levels of acetyl-STAT3 in 66 TNBC patient tumor tissues including four subtypes as indicated were assessed by fluorescent-immunohistochemistry (IHC) on a tumor tissue array. The levels of acetyl-STAT3 and cytokeratin was visualized by confocal microscopy. Representative images for each subtype are shown. Scale bar, 200 μ m.

(I) The levels of acetyl-STAT3 in primary or recurrent patient breast tumor tissues were assessed by fluorescent-IHC. The levels of acetyl-STAT3 and cytokeratin was visualized by confocal microscopy. Representative images from 5 paired samples are shown. Scale bar, 20 μ m.

The protein levels of acetyl-STAT3 or CPT1B in this figure were quantified by band intensity of western blotting using ImageJ software and normalized with the level of total STAT3 or β -actin as indicated. Statistical analysis, please also see Tables ST1H and ST2A.

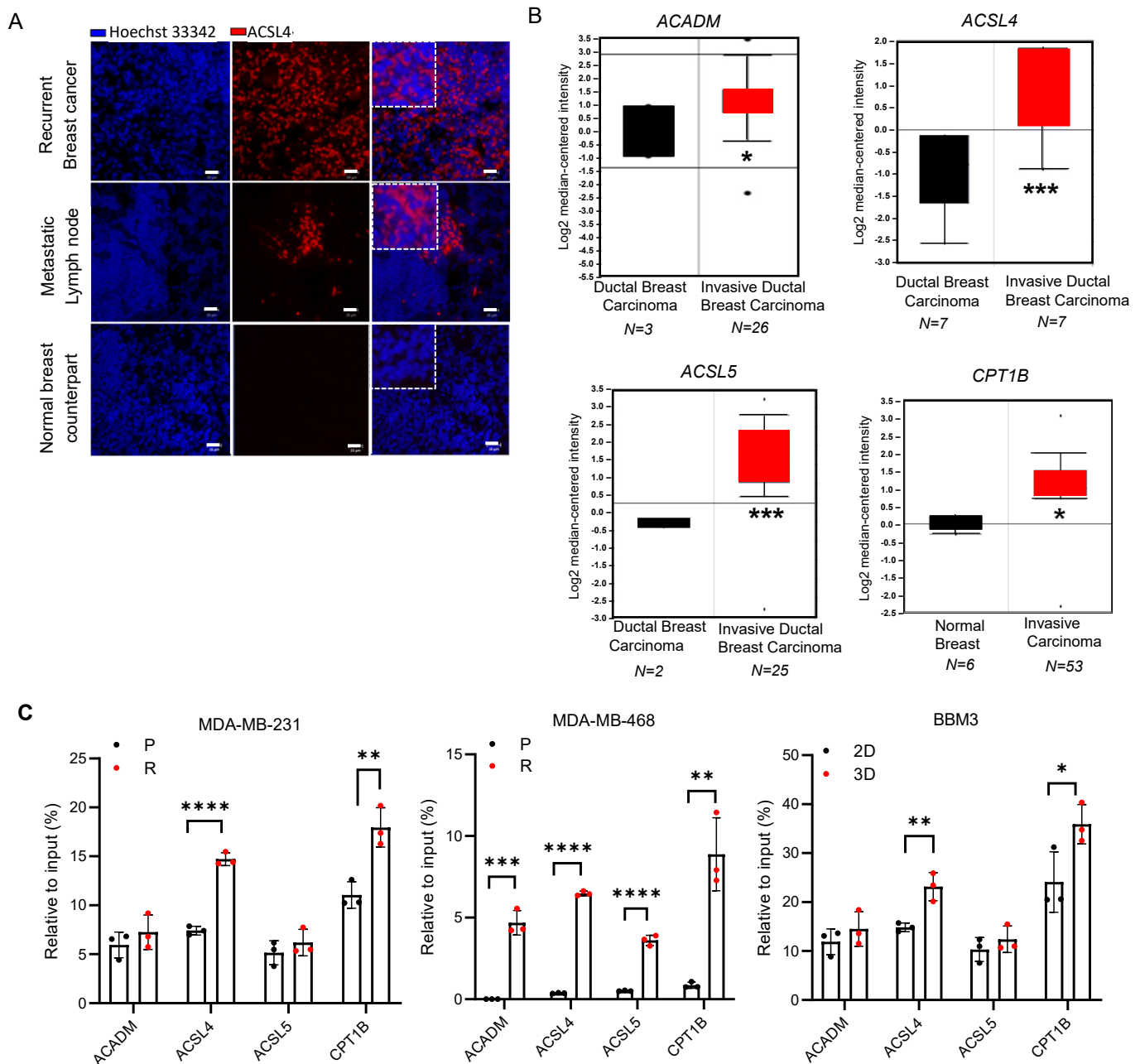


Figure S2. Elevated ACSL4 expression in invasive TNBC is mediated by acetyl-STAT3, related to Figure 2.

(A) Fluorescent-IHC images show that ACSL4 protein expression is upregulated in sections of recurrent TNBC tumors and nearby lymph nodes of the metastatic TNBC tumors. Representative images of three metastatic lymph nodes, breast tumor or normal tissue samples are shown. Scale bar, 20 μ m.

(B) Expression of lipid metabolic genes is upregulated in invasive TNBC breast tumors. The patient data was retrieved from Oncomine. Patient database: *CPT1B*, Finak Breast; *ACADM* and *ACSL5*, Radvanyi Breast; *ACSL4*, Schuetz Breast. Data shown are mean \pm SD. Two tailed, unpaired student's t test. *, $P < 0.05$; ***, $P < 0.005$.

(C) ChIP-qPCR for STAT3 at the promoter regions of lipid metabolic genes indicates STAT3 strongly regulated their expression in chemoresistant (R) MDA-MB231 and -468 cell lines or highly metastatic and cancer stem cell enriched (3D culture) BBM3 cell line compared to parental or 2D culture cells. ChIP assay of normal IgG (IgG) from the same sample was performed in parallel as a negative control. All ChIP-qPCR results were normalized with input DNA. Shown are mean \pm SD ($n=3$ biological replicates). Two tailed, unpaired student's t test. *, $P < 0.05$; **, $P < 0.01$; ***, $P < 0.005$; ****, $P < 0.001$. Statistical analysis, please also see Table ST11.

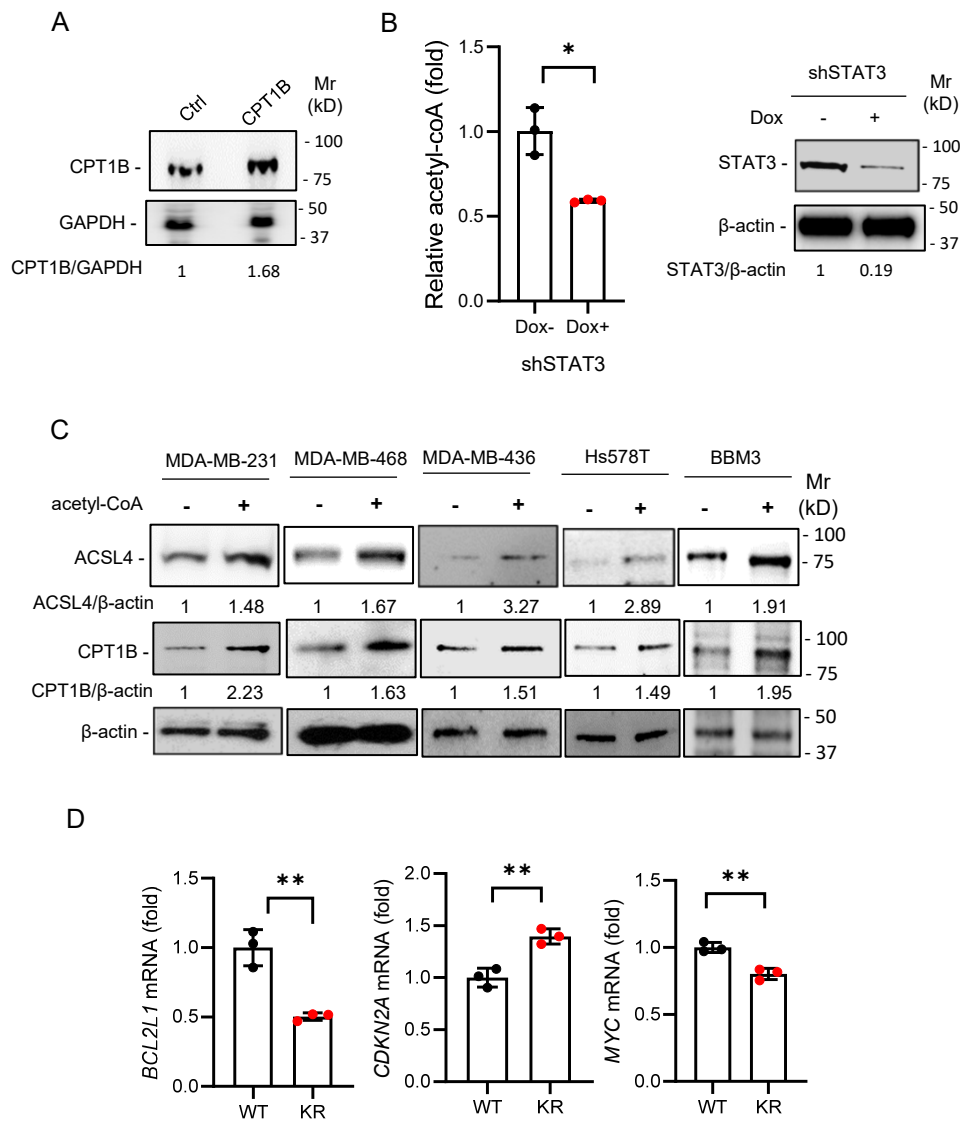


Figure S3. FAO/acetyl-CoA-acetyl-STAT3 pathway increases expression of ACSL4 and CPT1B, and acetyl-STAT3 is required for expression of genes involved in proliferation, related to Figure 3.

(A) The protein level of ectopic expression of CPT1B was detected by western blotting. GAPDH was examined as a loading control.

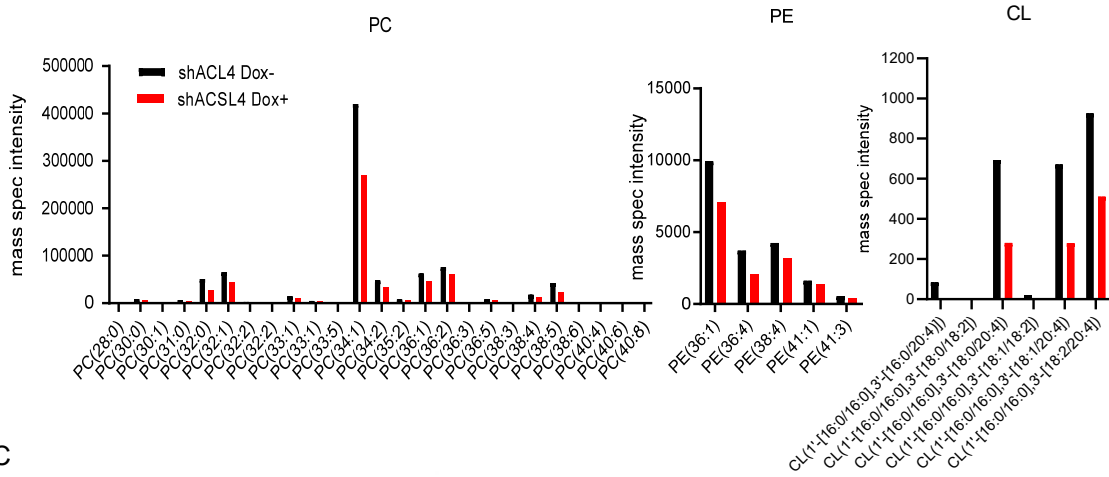
(B) Left panel, the level of acetyl-CoA was measured by acetyl-CoA fluorometric assay in chemoresistant MDA-MB-231-R cells after 5 d of STAT3 gene knockdown by doxycycline-induced shRNA (Dox+). Data shown are mean \pm SD; n=3 biological replicates; Two tailed and unpaired student's t test; *, P<0.05. Right panel, the protein levels of STAT3 after 5 d of gene knockdown were examined by western blotting.

(C) Acetyl-CoA was added to cultured TNBC cell lines as indicated for 16 h and the expression of ACSL4 and CPT1B was assessed by western blotting.

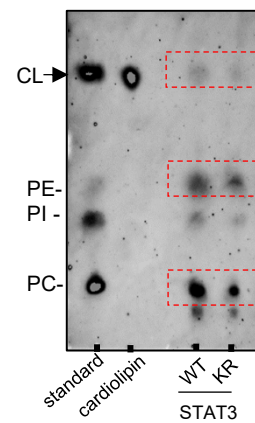
(D) Ectopic expression of KR-STAT3 inhibited expression of *BCL2L1* and *MYC* while increasing *CDKN2A*. The gene expression was examined by qPCR and the data shown are mean \pm S.D.; n=3 biological replicates; two-tailed and unpaired student's t test, **: P<0.01.

The protein levels of CPT1B, ACSL4, STAT3 or H3K27Ac in this figure were quantified by band intensity of western blotting using ImageJ software and normalized with β -actin or GAPDH as indicated. Statistical analysis, please also see Table ST1J.

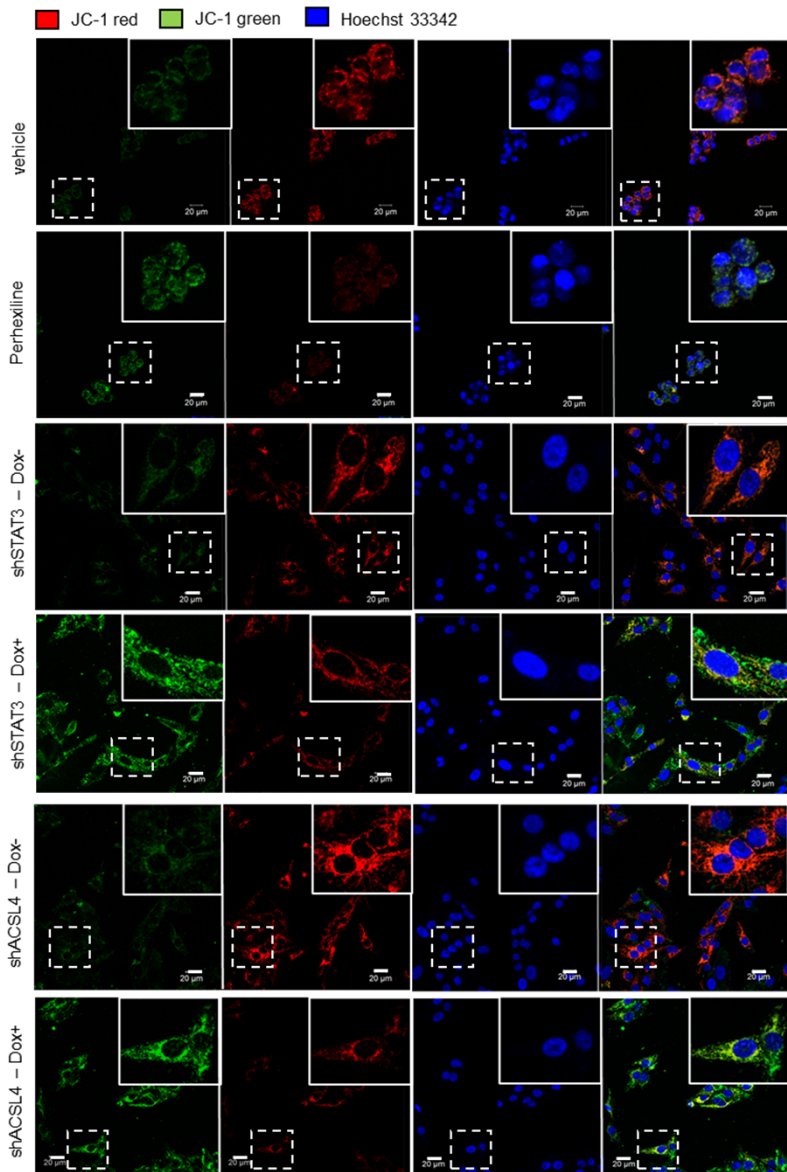
A



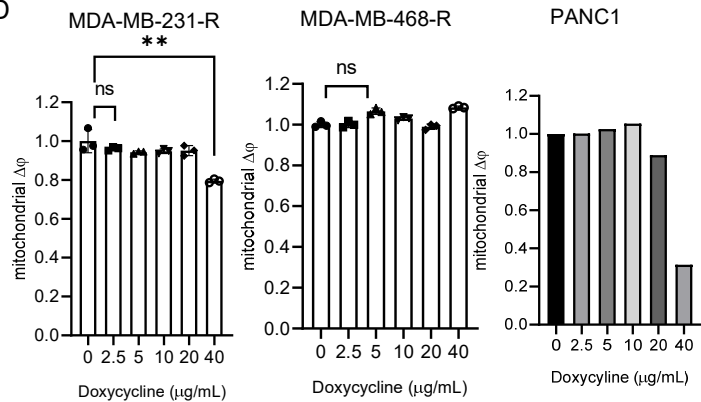
B



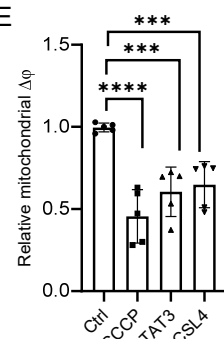
C



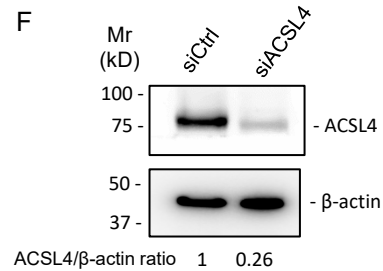
D



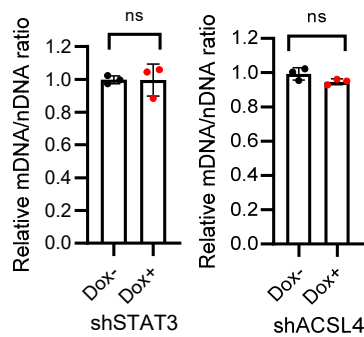
E



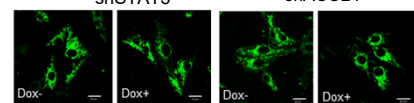
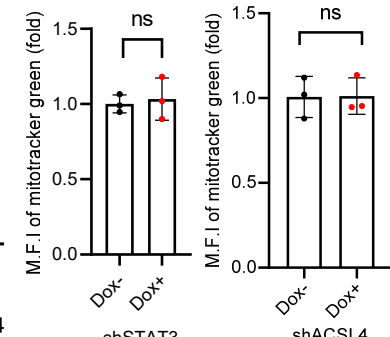
F



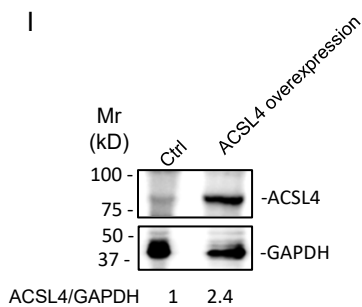
G



H



I



J

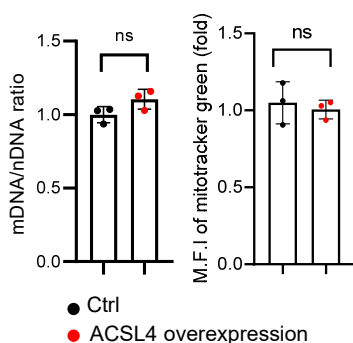


Figure S4. ACSL4-mediated phospholipid biogenesis increases mitochondrial $\Delta\psi$, but not mitochondrial mass, related to Figure 4.

(A) The levels of phosphatidylcholines (PC), phosphatidylethanolamines (PE) and cardiolipin (CL) content in chemoresistant MDA-MB-231 (MDA-MB-231-R) cells with (Dox+) or without (Dox-) ACSL4 gene knockdown (shACSL4) were detected and quantified by mass spectrometry.

(B) The mitochondrial membranes were isolated from the chemoresistant TNBC cells expressing WT-STAT3 or KR-STAT3. Phospholipid content was analyzed by TLC analysis. Data shown is the representative image from three independent experiments (n=3 biological replicates).

(C) MDA-MB-231-R cells were treated with vehicle or 10 nM of perhexiline for 16 h or doxycycline to induce STAT3 and ACSL4 knockdown for 5 d. Mitochondrial membrane potential was visualized by JC-1 staining and microscopy. The representative images of three samples (n=3) are shown. Scale bar, 20 μ m.

(D) The changes of mitochondrial membrane potential (mitochondrial $\Delta\psi$) in MDA-MB-231-R, MDA-MB-468-R and PANC1 cells after 5 d incubation with different concentrations of doxycycline as indicated. The mitochondrial membrane potential (mitochondrial $\Delta\psi$) was measured and quantified by flow cytometry. For MDA-MB-231-R, MDA-MB-468-R cells, data shown are mean \pm SD (n=3 biological replicates). Two tailed, unpaired student's t test. ns, not significant. **, P<0.01. For PANC1 cells, data shown are mean of the duplicated samples (n=2 biological replicates).

(E) The mitochondrial membrane potential (mitochondrial $\Delta\psi$) was measured by JC1 staining in MDA-MB-231-R cells with siRNA-mediated gene knockdown of STAT3 (siSTAT3), ACSL4 (siACSL4) or CPT1B (siCPT1B) for 5 d. The relative fluorescence was measured and quantified by flow cytometry. Shown are the mean \pm SD (n=5 biological replicates). Two tailed, unpaired student's t test. ***, P<0.005; ****, P<0.001.

(F) The protein level of ACSL4 after 5 d of siRNA-mediated gene knockdown in MDA-MB-231-R cells was assessed by western blotting. The protein level of ACSL4 was quantified by the protein band intensity and normalized with β -actin.

(G and H) The mitochondrial mass was measured by mitoDNA (mDNA) content (G) and MitoTracker Green (H) in the cells with (Dox+) or without (Dox-) STAT3 or ACSL4 knockdown in MDA-MB-231-R cells. (G) mDNA was examined by qPCR and normalized by nuclear DNA (nDNA). (H) MitoTracker Green was used to label mitochondria in the same cells described above and the mean of fluorescent intensity (M.F.I) was assessed and quantified by confocal microscopy and Zen software (Zeiss). Shown are mean \pm SD (n=3 biological replicates). Two tailed, unpaired student's t test. ns, not significant. The representative images of three samples are shown below the bar graph. Scale bar, 20 μ m.

(I) The protein level of ectopic expression of ACSL4 (ACSL4 overexpression) was determined by western blotting. The protein levels of ACSL4 were quantified by the protein band intensity and normalized with GAPDH.

(J) The mitochondrial mass was measured by mitoDNA (mDNA) content and MitoTracker Green in MDA-MB-231 cells with control or ectopic expression of ACSL4. mDNA was examined by qPCR and normalized by nuclear DNA (nDNA) (left panel). Mitotracker Green was used to label mitochondria in the same cells described above and the mean of fluorescent intensity (M.F.I) was examined and quantified by confocal microscopy and Zen imaging software (right panel). Shown are mean \pm SD (n=3 biological replicates). Two tailed, unpaired student's t test. ns, not significant.

Statistical analysis, please also see Table ST1K.

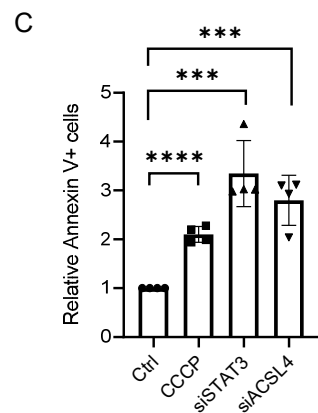
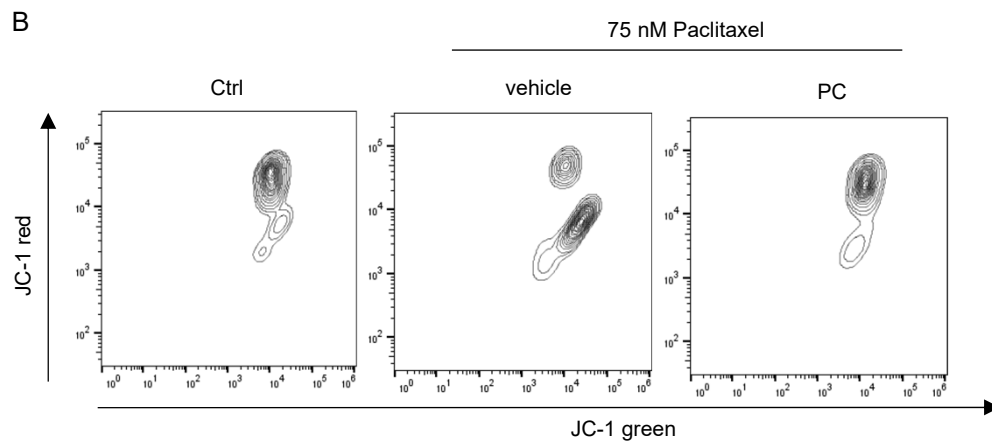
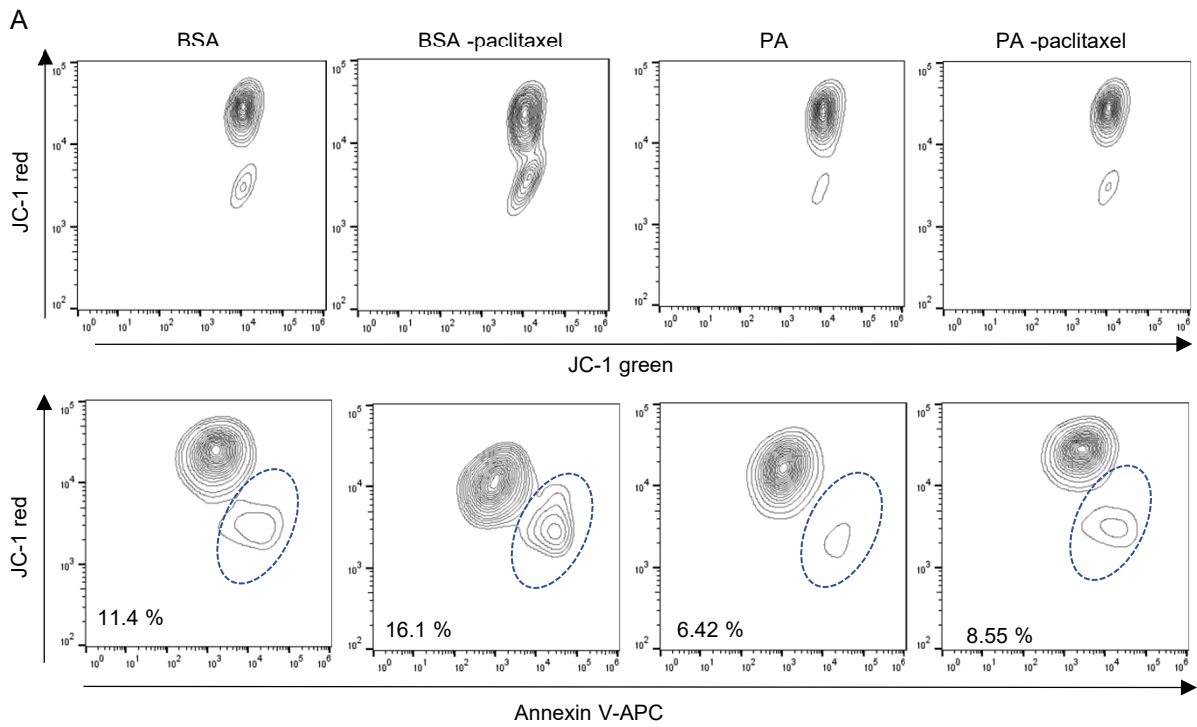


Figure S5. Flow cytometric analysis reveals FAO-STAT3 attenuated paclitaxel-induced apoptosis through increased phospholipid biogenesis, related to Figure 5.

(A) BSA or 50 μ M of palmitate (PA) in BSA was added to parental MDA-MB-231 cell culture for 3 d before paclitaxel (50 nM) was added to induce apoptosis for 24 h. Mitochondrial membrane potential was examined by JC1 staining and apoptosis was monitored by APC-Annexin V staining. Fluorescence of JC1 (upper panels) and JC1 coupled Annexin-V (lower panels) were detected by a flow cytometry. The mean of fluorescent intensity was quantified by FlowJo software. JC1-red^{low}Annexin-V⁺ cells were considered apoptotic cells (blue dash line). Data shown is representative of 3 independent experiments (n=3 biological replicates).

(B) Mitochondrial membrane potential were measured by JC1 after MDA-MB-231-R cells were treated with paclitaxel (75 nM) with in the presence of either vehicle or 50 μ M PC phospholipids for 48 h or left untreated as a control (Ctrl). Flow cytometry was used for the data analysis. The mean of fluorescence intensity (MFI) of JC1 red / JC1 green was quantified by FlowJo software. Data shown is representative of 3 independent experiments (n=3 biological replicates).

(C) The apoptosis were measured by Annexin-V/PI staining in MDA-MB-231-R cells with siRNA-mediated gene knockdown of STAT3 or ACSL4 for 5 d. The relative fluorescence was measured and quantified by flow cytometry and FlowJo software. Shown are the mean \pm SD (n=4 biological replicates). Two tailed, unpaired student's t test. ***, P<0.005; ****, P<0.001. Statistical analysis, please also see Table ST1L.

Figure S6. Cas9-mediated KO of genes important for FAO reduces mitochondrial membrane lipids and chemoresistant TNBC tumor growth, related to Figure 6.

(A) The protein levels of STAT3 (left panels) or ACSL4 (right panels) in the individual xenograft tumor shown in Figure 6 were assessed by western blotting. The protein levels of STAT3 or ACSL4 were quantified by band intensity of western blotting and normalized with β -actin. The relative protein levels in the tumors with gene knockdown (Dox+) were further normalized with the mean of the protein levels in the tumors without gene knockdown (Dox-).

(B) The transfection efficiency of CRISPR-Cas9 KO plasmid (GFP+) for STAT3, ACSL4 or CPT1B gene knockout (KO) in MDA-MB-231-R cells was examined by flow cytometry after 3 d transfection. GFP positive (Cas9-sgRNA-GFP) cells were used for establishing xenograft tumors.

(C) The protein levels of STAT3, ACSL4 or CPT1B in the STAT3, ACSL4 or CPT1B KO MDA-MB-231-R cells were examined by western blotting after 3d transfection. The protein levels were quantified normalized with β -actin.

(D) Upper panel, mock, STAT3 or ACSL4 KO chemoresistant MDA-MB-231-R cells were orthotopically implanted in the mammary fat pad of female NSG mice. Tumor growth kinetic was measured by tumor size and the data are shown as mean \pm SEM; n=5 mice in each group; Two-way ANOVA; ****, P<0.001. Lower panels, The protein levels of STAT3 or ACSL4 in the individual xenograft tumor of mock, STAT3 KO or ACSL4 KO were assessed by western blotting. The protein levels of STAT3 or ACSL4 in individual tumor were measured and quantified by the band intensity of western blotting and normalized with β -actin. The relative protein levels in the tumors with gene knockout (KO) were further normalized with the mean of the protein levels in the mock tumors.

(E and F) Fluorescent-IHC of tumor sections from (D). (E) The levels of Ki67 and cleaved caspase 3 were visualized by IHC on the tumor sections. Hoechst 33342 was used for nuclear counter staining. The representative images of five samples are shown. Scale bar, 50 μ m. (F) The level of Ki67 or cleaved caspase 3 in the individual tumor was quantified by Zen software (Zeiss) and the mean of the fluorescent intensity was shown in bar graphs. Hoechst 33342 was used for nuclear counter staining. Data are shown as mean \pm S.D.; n=5 tumors; Two tailed and unpaired student's t test. ***, P<0.005; ****, P<0.001.

(G) The levels of PC, PE and CL in the mitochondrial membranes from the orthotopically implanted MDA-MB-231-R tumors as described in (E) were analyzed by TLC and quantified by ImageJ software. Data are shown as mean \pm S.D.; n=5 individual tumors; Two tailed and unpaired student's t test. ****, P<0.001.

(H) Upper panel, mock or CPT1B KO chemoresistant MDA-MB-231-R cells were orthotopically implanted in the mammary fat pad of female NSG mice. Tumor growth kinetic was measured by tumor size and the data are shown as mean \pm SEM; n=4 mice in each group; Two-way ANOVA; ****, P<0.001. Lower panel, the protein levels of CPT1B in the individual xenograft tumor of mock or CPT1B KO were assessed by western blotting. The protein levels of CPT1B were measured and quantified by band intensity of western blotting and normalized with β -actin. The relative protein levels in the tumors with KO were further normalized with the mean of the protein levels in the mock tumors.

(I) The levels of PC, PE and CL in the mitochondrial membranes from the orthotopically implanted MDA-MB-231-R tumors as described in (H) were analyzed by TLC and quantified by ImageJ software. Data are shown as mean \pm S.D.; n=4 individual tumors; Two tailed and unpaired student's t test. ***, P<0.005; ****, P<0.001.

(J) Ferroptosis was not induced by gene knockdown of ACSL4 and STAT3. ACSL4 or STAT3 gene was knockdown by doxycycline-induced shRNA (Dox+) in MDA-MB-231-R cells. Ferroptosis was measured by C11-BODIPY staining. RSL3, a ferroptosis activator, was used as a positive control. Relative mean fluorescence intensity (M.F.I) was measured by flow cytometry and normalized to the control cells (Dox-). Shown are mean \pm SD. n=3 biological replicates. Two tailed student's t test. ns, not significant; ***, P<0.005; ****, P<0.001.

Statistical analysis, please also see Table ST1M.

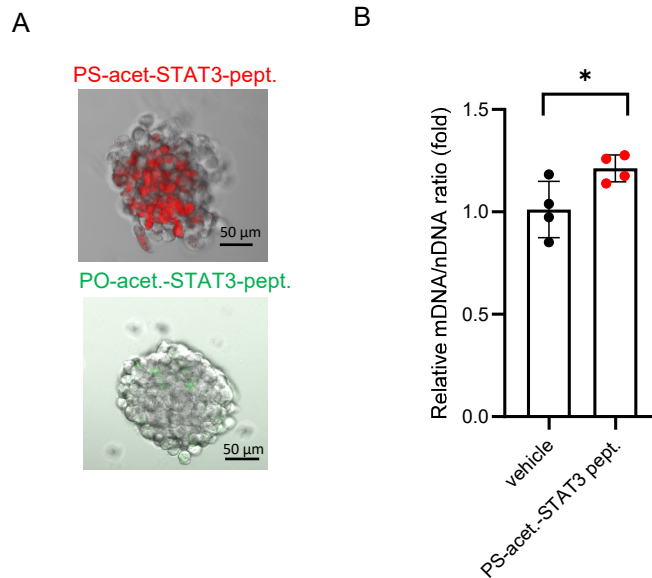


Figure S7. The tumor sphere penetration and the effects on mitochondrial mass by PS-acet.-STAT3 pept., related to Figure 7

(A) PS-acet.-STAT3 pept. but not PO-acet-STAT3 pept. was able to penetrate into patient primary TNBC tumor spheres. 10 μg of fluorescent labeling peptide was incubated with TNBC patient primary tumor spheres for 2 h and the peptide penetration was determined by fluorescent microscopy. TAMRA-PS-acet.-STAT3 pept. (red), FAM-PO-acet.-STAT3 pept. (green). Scale bar, 50 μm .

(B) The mitochondrial DNA (mDNA) content in the individual tumor tissues treated with vehicle or PS-acet.-STAT3 pept. was examined by qPCR and normalized by nuclear DNA (nDNA). Data shown are mean \pm SD. $n=4$ biological replicates; Two tailed and unpaired student's t test, *, $P<0.05$. Statistical analysis, please also see Table ST1N.

Suppl. Table 3. Related to STAR Methods.

The sequences of oligo primers used for qPCR, ChIP assays or generating shRNAs.

The sequences of oligo primers used for qPCR		
number	name	sequence 5' to 3'
1	hBCL2L1 F	GTCCTCACTCCCAGTCCAA
2	hBCL2L1 R	GCTGAGGCCATAAACAGCC
3	hMYC F	CACCGAGTCGTAGTCGAGGT
4	hMYC R	GCTGCTTAGACGCTGGATTT
5	hACTB F	AGGCACCAGGGCGTGAT
6	hACTB R	GCCCACATAGGAATCCTTCTGAC
7	hCDKN2A F	CTCGTGCTGATGCTACTGAGGA
8	hCDKN2A R	GGTCGGCGCAGTTGGGCTCC
9	hGAPDH F	GTCTCCTCTGACTTCAACAGCG
10	hGAPDH R	ACCACCCTGTTGCTGTAGCCAA
11	hACSL4 F	AGGACATTTAAAACGCTATGGCA
12	hACSL4 R	GTCCCAAGGCTGTCCTTCTT
13	hCPT1B F	CTGCCTTTACTTGGTCTCCA
14	hCPT1B R	GCTGGAGATGTGGAAGAAGA
15	human B2M Fwd	TGCTGTCTCCATGTTTGATGTATCT
16	human B2M Rev	TCTCTGCTCCCCACCTCTAAGT
17	human tRNA ^{Leu} Fwd	CACCCAAGAACAGGGTTTGT
18	human tRNA ^{Leu} Rev	TGGCCATGGGTATGTTGTTA
The sequences of oligo primers used for chromatin immunoprecipitation (ChIP) assay		
number	name	sequence 5' to 3'
1	ACADM F	ACATATTGGAGGCCGAAACA
2	ACADM R	GCATACGCAGTTTGTGTCAGTTC
3	ACSL4 F	GCACCCAAGTTGAAGAGGAAA
4	ACSL4 R	GAAAGCTGGAAATAGCGTGGT
5	ACSL5 F	GTAATGATGCACACAGGCACC
6	ACSL5 R	CCAGAGCGTTCTTGTGTCAGTCA
7	CPT1B F	GGGTCTGCTTCATACCCCCA
8	CPT1B R	GAGCAGCAGCAGAAAGTACC
The sequences of the oligos used for generating shRNAs		
number	name	sequence 5' to 3'
1	shACSL4 Forward	CCGGGGAAATTTGCAGCTTCCAATGCTCGAGCATTGGA AGCTGCAAATTTCTTTTT
2	shACSL4 Reverse	AATTA AAAAGGAAATTTGCAGCTTCCAATGCTCGAGCAT TGGAAGCTGCAAATTTCC
3	shSTAT3 Forward	CCGGGCCCTCGTATGAGGGTGTATACTCGAGTATACAC CCTCATACGAGGGCTTTTT
4	shSTAT3 Reverse	AATTA AAAAGCCCTCGTATGAGGGTGTATACTCGAGTAT ACACCCTCATACGAGGGC